Antidepressant drugs diversely affect autophagy pathways in astrocytes and neurons - dissociation from cholesterol homeostasis

Running Title: Autophagy is induced by antidepressants

Jürgen Zschocke* Ph.D., Nicole Zimmermann M.Sc., Barbara Berning, Vanessa Ganal, Florian Holsboer Ph.D., M.D. and Theo Rein Ph.D.

Max Planck Institute of Psychiatry, Kraepelinstr. 2-10, 80804 Munich, Germany

*Corresponding author Jürgen Zschocke, Ph.D.

Max Planck Institute of Psychiatry

Kraepelinstr. 2-10

80804 Munich

Germany

Phone: +49 89 30622 227

FAX: +49 89 30622 610

Email: zschocke@mpipsykl.mpg.de

Abstract

In search for antidepressants' mechanisms of action beyond their influence on monoaminergic neurotransmission, we analyzed the effects of three structurally and pharmacologically different antidepressants on autophagic processes in rat primary astrocytes and neurons. Autophagy plays a significant role in controlling protein turn-over and energy supply. Both, the tricyclic antidepressant amitriptyline (AMI) and the selective serotonin re-uptake inhibitor citalopram (CIT) induced autophagy as mirrored by pronounced up-regulation and cellular redistribution of the marker LC3B-II. Redistribution was characterized by formation of LC3B-II positive structures indicative of autophagosomes which associated with acidic vacuoles in a time-dependent fashion. Deletion of Atg5 representing a central mediator of autophagy in mouse embryonic fibroblasts led to abrogation of AMI-induced LC3B-I/II conversion. In contrast, venlafaxin, a selective serotonin and noradrenaline reuptake inhibitor, did not promote autophagic processes in either cell type. The stimulatory impact of AMI on autophagy partly involved class III PI3 kinase-dependent pathways since 3-methyladenine slightly diminished AMI effects. Autophagic flux as defined by autophagosome turnover was vastly undisturbed, and degradation of long-lived proteins was augmented upon AMI treatment. Enhanced autophagy was dissociated from drug-induced alterations in cholesterol homeostasis. Subsequent to AMI and CIT mediated autophagy induction, neuronal and glial viability decreased, with neurons showing signs of apoptosis. In conclusion, we report that distinct antidepressant promote autophagy in neural cells, with important implications on energy homeostasis.

Keywords: autophagosome, lysosome, amitriptyline, citalopram, class III PI3 kinase, mitochondria, antidepressants

List of abbreviations: 3-MA *3-methyladenine*, **AD** *antidepressant drug*, **AMI** amitriptyline, **Atg** *autophagy-related gene*, **AV** *acidic vacuole*, **BafA** *bafilomycin A1*, **CAD** *cationic amphiphilic drug*, **CIT** *citalopram*, **HMG-CoA** *3-hydroxy-3-methylglutaryl-coenzyme A*, **LC3** *microtubule-associated protein light chain 3*, **LDH** *lactate dehydrogenase*, **mTOR** *mammalian target of rapamycin*, **NP-C** *Niemann-Pick type C*, **PI3 kinase** *phosphatidyl-inositol-3 kinase*, **ROS** *reactive oxygen species*, **VEN** *venlafaxin*, **VPA** *valproate*, **TCA** *tricyclic antidepressant,* **UPR** *unfolded protein response*

Introduction

Major depressive disorder (MDD) is a severe medical condition that raises the need for elaborated pharmacological interventions. Current generations of antidepressants (ADs) are commonly assumed to share as principle of action the influence on transmitter circuits of neuronal networks. In addition to neurons, glia cells come into focus as significant mediators of ADs' therapeutic effects (Czeh et al. 2006).

Tricyclic antidepressants (TCAs) were introduced in the 1950s for treatment of MDD. The known molecular targets of TCAs range from noradrenaline and serotonin transporters to alpha$_2$ adrenergic, nicotinic, muscarinic and histaminergic receptors. In most cases, they exert an inhibitory effect on the respective targets (Owens et al. 1997).

More recently developed ADs were designed to specifically impede the activity of neurotransmitter transporters, and are thus called selective serotonin re-uptake inhibitors (SSRIs) or selective serotonin/noradrenalin-reuptake inhibitors (SSNRIs). However, mounting evidence suggests the existence of various additional targets for both, TCAs and SS/NRIs, which may be either supportive for the therapeutic effects, or at the contrary, trigger adverse events (Carvalho et al. 2010; Herr et al. 2003; Nothdurfter et al. 2010; Perisic et al. 2010).

First, ADs interfere with signaling pathways including MEK/p38/c-Jun kinases as well as with a multitude of second messenger systems (Hisaoka et al. 2007; Paez-Pereda 2005). Second, processes involving carbohydrate and lipid metabolism are frequently altered in response to AD exposure (Raeder et al. 2006a; Raeder et al. 2006b). Third, TCAs in particular impact on biophysical properties of cellular membranes due to their cationic amphiphilic structure that allows complex interactions with phospholipid bilayers. As a consequence, membrane fluidity, lipid composition, and membrane protein activity might be changed. Moreover, phospholipid particles might accumulate in lysosomal lamellar bodies (Alakoskela et al. 2009; Xia et al. 2000). In 1990, a study by Rodriguez-Lafrasse elucidated the morphology of imipramine treated fibroblasts as resembling that of cells that originate from Niemann-Pick type C (NP-C) disease (Rodriguez-Lafrasse et al. 1990). NP-C is one of the lysosomal storage disorders characterized by high levels of unesterified cholesterol and sphingolipids in late endosomes and lysosomes (Chang et al. 2005). Importantly, a phenomenon termed autophagy has recently been reported to be associated with Niemann-Pick type C pathology in an NP-C1$^{-/-}$ mouse model (Liao et al. 2007).

Autophagy is an evolutionary conserved mechanism that promotes survival of stressed or starved cells by eliminating damaged macromolecules, organelles, protein aggregates, and by providing nutrients (Glick et al. 2010). Contrasting cell survival functions, extensive or impaired autophagic activity might result in type II cell death that is different from caspase-mediated apoptosis, also called type I cell death (Gozuacik and Kimchi 2004). In distinct settings, autophagy is thought to act as a back-up system to execute cellular death (Shimizu et al. 2004). Several consecutive steps constitute the progression of autophagy, which are operated by a cascade of autophagy-related (Atg) genes. Initially, a phospholipid isolation membrane encloses cytoplasmic components building an autophagosome. Fusion of the membrane of the autophagosome with lysosomes leads to the degradation of engulfed material by lysosomal hydrolases producing smaller units that are subsequently recycled (Huang and Klionsky 2002; Mehrpour et al. 2010). Most tissues maintain a basal autophagic flux under normal physiological conditions to ensure turn-over of long-lived proteins and organelles. Autophagic activity is regulated by multiple pathways including Akt/mTOR-, class III PI3 kinase (Vps34)/beclin1-, CaMKK-β/LKB1/AMP kinase- and Raf-1/MEK/ERK-dependent signaling cascades (Corcelle et al. 2009).

Up to date, it is unclear whether there is a direct causal link between cholesterol accumulation in vacuole compartments and increased autophagy in NP-C cells, and whether autophagy might offer protection to cholesterol-burdened cells or rather drive cell elimination through type II cell death.

Strikingly, the additional effects of some ADs described above, encompassing modulation of signaling pathways, cholesterol homeostasis and phospholipid interaction,

largely coincide with molecular factors affecting autophagy. Therefore, we investigated the impact of different ADs on autophagic processes in primary astrocytes and neurons. Additionally, we elucidated possible mechanisms underlying autophagy induction that involves cholesterol homeostasis and signaling pathways. Finally, we tested for functionality of autophagy by means of alterations in cellular protein and organelle turnover. Although disentangling the relevance of autophagy for the beneficial and adverse side effects of ADs will be a far reach, elucidating AD actions beyond monoamines will set the stage for a more thorough understanding of the mechanisms of action for this class of drugs.

Materials and Methods

Drugs

Valproate (VPA), amitriptyline (AMI), citalopram (CIT), bafilomycin A (BafA), pepstatin A, E-64d, 3-methyladenine (3-MA) and vitamin E (VitE) were purchased from Sigma (Deisenhof, Germany). Venlafaxine (VEN) was an industrial donation (Wyeth Pharma GmbH, Münster, Germany). Stock solutions of the drugs were prepared by dissolving the substances in distilled water (VPA, AMI, CIT, VEN, 3-MA) or in 100% ethanol (BafA, pepstatin A, E-64d, VitE).

Cell line

ATG5 wildtype and knockout mouse embryonic fibroblasts were a kind gift of N. Mizushima (Kuma et al. 2004). Cells were maintained in DMEM supplemented with 10% FCS (all from Invitrogen).

Preparation of rat primary astrocytes and neurons

Neocortical neurons were enriched from embryonic d 18 rat brains (Sprague Dawley, Charles River, Sulzfeld, Germany). Astrocytic cultures were initiated from postnatal d1 animals. Dams were narcotized by isofluran inhalation, and newborns were physically decapitated. Preparation and cultivation of cells was as described before (Bayatti et al. 2003; Franke et al. 1998).

Transfection of primary astrocytes and neurons

Transfection of primary astrocytes and neurons with the pEGFP-LC3 plasmid (Addgene, originally provided by T.Yoshimori) was performed using the Nucleofactor transfection reagent and electroporator according to the manufacturer's protocol (Amaxa, Cologne, Germany). Briefly, astrocytes of the second passage were trypsinized, and subsequently 2 x 10^6 cells were applied to electroporation with 5 µg of plasmid DNA. Cells were seeded in a 24-well plate and allowed to recover for 24 h in MEM/10% horse serum. After 24 h, cell culture medium was changed to MEM/HAM F-12 (1:1) N2-supplemented (1%) medium. Cells were stimulated with the indicated concentrations of AMI for 12 h or 24 h. Similar to astrocytes, 5 x 10^4 neurons were transfected with 500 ng

plasmid, and processed in analogy to astrocytes, except using Neurobasal medium after recovery.

UPR Reporter Gene Assay

Transfection of astrocytes was as described before, and reporter gene assays were in accordance with Schulke et al. (Schulke et al. 2010). Utilized vectors included the constitutively active SV40-driven Gaussia-KDEL for normalization of transfection efficiency and ERSE-I-luciferase (Bouman et al. 2010). After transfection of 200 ng Gaussia-KDEL and 1 µg ERSE-I-Luciferase per 2 x 10^6 astrocytes, cells were allowed to recover for 48 h; medium was then changed to MEM/F12/N2 together with drug stimulation as specified in the result section.

Cell Viability Assays

Lactate dehydrogenase (LDH) assay – The release of LDH into the growth medium of astrocytes served as indicator for membrane disruption and cell death. The assay was carried out in accordance to the LDH cytotoxicity detection system (Clontech, Mountain View, CA) pursuant to the manufacturer's protocol. As negative control, empty wells were used with medium only; as positive control, 0.02% Triton X-100 was added to the assay medium 1-2 h prior to the assay.

MTT assay – Neurons were incubated in the presence of 0.5 mg/ml MTT reagent [tetrazole 3-(4,5-dimethylthiazol-2-yl-)-2,5-diphenyltetrazolium bromide] for 4 h at 37 ^oC with 5% CO_2. Read-out of MTT metabolism was as described previously (Moosmann et al. 2001). ADs interfered with the MTT assay in astrocytes and produced artificial results;

therefore, the MTT was substituted by the LDH release assay (Berridge and Tan 1993; Liu et al. 1997).

TUNEL assay –TUNEL assay was performed following the Roche procedure. Cells on coated glass cover slips (see also immuno-fluorescence) were washed with PBS and fixed with 4% paraformaldehyde for 1 h. After rinsing with PBS, cells were permeabilized with 0.1% sodium citrate/0.1% Triton X-100 for 2 min on ice, and incubated with TUNEL reaction mix including terminal transferase for 60 min at 37 ^{o}C. Subsequent to three washes with PBS and mounting, cells were analyzed at 515 nm using a Zeiss Axioplan-2 fluorescence microscope.

Western Blot analysis

Protein extracts were obtained by lysing neural cells in buffer containing 21 mM Tris/HCl pH 6.8, 0.66% SDS and 3.33% sucrose, supplemented with protease inhibitor cocktail (Sigma). Western blot was performed as described previously (Perisic et al. 2010). The immuno-reactive bands were visualized using ECL detection reagent (Millipore, Billerica, MA, USA). The following primary antibodies were used: anti-LC3B (1:1000, #2775, Cell Signaling), anti-beclin1 (1:2000, #3738, Cell Signaling) anti-cleaved caspase-3 (1:500, # D175, Upstate) and anti-α actin (1:2500; #A2066, Sigma), anti-hsc70 (1:1000, # sc-7298, Santa Cruz).

Real-time PCR analysis

Total RNA was isolated from astroglial and neuronal cells according to the manufacturer's protocol of NucleoSpin RNA II (Macherey-Nagel, Germany). In total,

300 ng of purified RNA was reverse transcribed using random primers (Promega) and Omniscript Reverse Transcriptase (Qiagen). Based on the LightCycler® System (Roche Applied Science, Germany) and SYBR green detection (QuantiFast SYBR Green, Qiagen), quantitative assessments of HMG-CoA reductase and NPC2 cDNA levels were carried out. Beta-actin PCR was performed serving as endogenous control for normalization. The primers used are listed in Supplementary Table 1. Relative changes of gene expression were calculated using the comparative $\Delta\Delta C_T$ method (Livak and Schmittgen 2001).

Cholesterol determination

Cellular cholesterol concentrations were determined either in whole cell lysates or cytoplasmic fractions. Extracts for whole cell lysates were prepared using 50 mM Tris, pH 8.0, 2 mM $CaCl_2$, 80 mM NaCl and 1% Triton X-100. In case of fractionation, cells were washed with ice-cold PBS, trypsinized and pelleted by centrifugation. Cell pellets were resuspended 1 ml of homogenization buffer (50 mM Tris/HCl pH 7.9, 126 mM NaCl, 5 mM KCl). Homogenization was performed by using a Dounce homogenizer and a Branson sonicator (15-s pulsed bursts, 90% output). The homogenized sample was spun at 800 × *g* for 10 min at 4 °C. The obtained postnuclear supernatant was centrifuged for an additional 1 h at 4 °C and 100,000 × *g*. The supernatant, representing the cytoplasmic fraction, was directly processed for cholesterol determination. Free cholesterol was measured using the Amplex Red Cholesterol Assay (Invitrogen) according to the manufacturer. Per sample, an equivalent volume of 6 µg protein was subjected to the assay. Fluorometric readings were performed at 595 nm with a Tecan plate reader.

Measurement of long-lived protein turnover

Treatment regime of astrocytes and neurons was as described in the results section (Fig. 7A). At the last day of AMI treatment, cells were labeled with 2 µCi ^{3}H-leucine per well/12-well plate. After 24 h of labeling, cells were washed two times with MEM/F12/N2 and incubated with medium supplemented with 2.4 mM leucine. Four hours later, medium was changed again, and medium was collected after 8 h. In parallel, cells were lysed in buffer containing 10 mM Tris/HCl pH 8.0, 150 mM NaCl, 2 mM EDTA, 0.5% deoxycholate, 2% NP40. Medium and lysates were adjusted to 1% BSA used as a carrier protein and 20% trichloroacetic acid, incubated for 10 min on ice, and spun at 12.000 rpm for 10 min. Trichloroacetic acid-insoluble pellet was dissolved in 0.2 N NaOH at 60 °C. Total radioactivity from supernatant and dissolved pellet was measured by scintillation counting, and ratios of trichloroacetic acid-soluble/insoluble fractions per treatment condition were calculated.

Fluorometric quantification of lysosomes

The amount of acidic vacuoles was fluorometrically assessed at the cellular level. Medium of cells grown in 6-well plates was changed to fresh medium containing a 1:20,000 dilution of Lysotracker Red (LysoRed) and a 1:2000 dilution of CellTracker Green (all from Invitrogen), within the same well. The dye-supplemented medium was kept on cells for 30 min, and subsequently cells were allowed to recover in medium without dye. Subsequently, cells were trypsinized, and cell pellet was resuspended in 100 µl phenol-red-free medium and transferred to a 96-well plate. Readings were performed

at the appropriate wavelength with a Tecan plate reader using CellTracker Green for normalization to the cell number.

Cellular staining of free cholesterol

Cells grown on coated glass coverslips were washed with PBS, fixed with 3% paraformaldehyde in PBS for 20 min at RT, and rinsed with 1.5 mg glycine/ml PBS for 20 min. After quenching, cells were washed again with PBS and subsequently incubated with filipin staining solution (50 µg/ml filipin, 10% goat serum, 90% PBS) at RT for 2 h in the dark. Staining was completed by three additional PBS washes, and by mounting with Prolong antifade reagent (Invitrogen). The excitation wavelength was 351 nm.

Immunocytochemistry

Cells grown on poly-ornithin/laminin (all 0.1 mg/ml) coated glass coverslips were briefly washed with PBS and fixed at room temperature for 10 min with 4% formaldehyde in PBS. Cells were permeabilized by rinsing two times (10 min) with PBS containing 0.05% saponin. After permeabilization, cells were incubated in blocking solution (10% goat serum in PBS) for 60 min. The coverslips were treated overnight at 4 ^{o}C with LC3B, GFAP (# 20334, Dako) or MAP2 (# M2320, Sigma) primary antibody (all 1:200 in PBS/0.05% Triton and 10% goat serum). After three washes with PBS/0.05% Triton, cells were incubated with the secondary antibody for 1 h at room temperature (IgG conjugated with Cy2, Dianova, diluted 1:200 in PBS/0.05% Triton). Finally, cells were washed three times in PBS, nuclei were counterstained with 5 µg/ml 4',6-diamidino-2-phenylindole (DAPI), and slides were mounted with Prolong Antifade® (Molecular

Probes). Cells were visualized by using either a Leica confocal laser scanning microscope (TCS NT) or Olympus DP50 microscope.

Statistics

Experiments with statistics were generally carried out three times with similar results. Data were collected from independent experiments, and significance between treatment and control groups was further analyzed using the *Student's t*-test.

Results

We analyzed the impact of three different ADs, the TCA amitriptyline (AMI), the SSRI citalopram (CIT) and the SNRI venlafaxine (VEN) on autophagy and associated processes. Since the mood-stabilizer valproic acid (VPA) has recently been reported to induce autophagy in glioma cells, we also included VPA that is frequently administered as augmentation therapy of MDD. For all ADs tested, drugs were applied at concentrations between 1 and 10 μM. According to studies in rodents, similar and higher concentrations are achieved in brain tissue that generally shows enrichment of certain drugs as compared to serum levels (Glotzbach and Preskorn 1982; Holladay et al. 1998). We used primary astrocytes as well as neurons from cerebral hemispheres to analyze possible cell type specific differences.

Antidepressants exhibit differential effects on vacuolization in astrocytes and neurons - We first evaluated sub-cellular features of drug-treated astrocytes and neurons focusing on vacuolar structures. In case of AMI and CIT exposure astrocytes developed several layers of perinuclear acidic vacuoles (AVs) occupying a significant part of the cytosol, whereas VEN and VPA did not promote vesicle formation (Fig. 1). Overall shape of cells was not grossly changed after incubation with AMI and CIT, while some cytoskeletal rearrangements occurred as reflected by GFAP staining. This is in basic agreement with the observation that the TCA desipramine does not markedly induce cellular changes of C6 glioma cells (Donati et al. 2001). When cells were co-treated with 20 nM bafilomycin A (BafA), an inhibitor of the proton pump V-ATPase that acidifies various organelles, vacuolization was disrupted (Fig. S1). Further, AVs were enriched in free cholesterol as shown by filipin staining (Fig. 2). In neurons, formation of AVs upon treatment with AMI or CIT could also be observed. Using a quantitative fluorometric technique to evaluate the potency of the applied drugs to promote AV formation, we found AMI to be more effective than CIT at 1 μM and 5 μM (Fig. 3A), while both substances showed a similar effect size at the highest concentration of 10 μM in astrocytes. Time course experiments revealed a rapid onset of AV formation as early as 12 hours after commencing exposure with AMI or CIT (10 μM) (Fig. 3B). In neurons, the magnitude of increase in LysoRed signal was ~5-fold lower as compared to astrocytes. VEN and VPA did not promote the formation of AVs in either cell type (Fig. 3C). Together, AMI and CIT increase AVs in a dose, time- and cell type dependent fashion.

AMI, but not CIT, modulates cholesterol biosynthesis and trafficking pathways - We next asked whether the appearance of free cholesterol in AVs after AMI/CIT exposure is related to an increased cholesterol biosynthesis or to altered activity of genes responsible for cholesterol trafficking. The expression level of the rate limiting enzyme of cholesterol biosynthesis, HMG-CoA reductase, is a well-established predictor of cellular changes in cholesterol homeostasis. Short-term treatment with AMI (10 μM, 12 h) led to a subtle elevation of HMG-CoA reductase mRNA levels, with astrocytes responding stronger than neurons, while no effects were observed after 72 h (Fig. 4A). In contrast, CIT did not affect HMG-CoA reductase transcription in astrocytes, and only faintly in neuronal cultures. Since HMG-CoA reductase expression changes could impact on cellular cholesterol concentrations, we determined the levels of cytoplasmic and total cholesterol. Cytoplasmic levels of free cholesterol (Fig. 4C) were modestly elevated in astrocytes after treatment with AMI, but not CIT (72 h, 10 μM each), possibly reflecting the differential effect of these drugs on HMG-CoA reductase expression. There were no changes in total cholesterol, neither in astrocytes nor in neurons (Fig. 4D). In general, cytoplasmic cholesterol of untreated astrocytes made up for ~ 18% of total cholesterol (4.17 ± 0.71 μg cytoplasmic cholesterol/mg protein versus 24.4 ± 3.5 μg total cholesterol/mg protein). Due to the under-representation of the cytoplasmic cholesterol fraction, the observed two-fold increase of cytoplasmic cholesterol levels after AMI incubation is apparently not mirrored in total cholesterol changes.

Since accumulation of cholesterol in AVs could be also explained by aberrant cholesterol trafficking, we analyzed a key regulator of cholesterol shuttling, the Niemann-Pick type C 2 gene (NPC2) whose gene product coordinates the egress of free cholesterol

from lysosomes for delivery to the endoplasmatic reticulum and other subcellular compartments (Xu et al. 2008). Real-time PCR revealed time-dependent up-regulation of NPC2 coding mRNA by AMI (Fig. 4B), pointing to an intact molecular response to elevated cytoplasmic cholesterol levels. Conversely, CIT, that did not affect cholesterol synthesis, also did not alter the expression of NPC2. Taken together, overall cholesterol levels are not altered, and the drug-induced accumulation of free cholesterol in lysosomes is not generally linked to enhanced cholesterol synthesis or to defective NPC2 gene regulation.

AMI and CIT enhance expression of autophagic markers - Cellular vacuolization as observed in the aetiopathology of NP-C has recently been reported to come along with autophagy in cell culture and animal models (Liao et al. 2007; Pacheco et al. 2007). Autophagic processes are accompanied by pre- and post-translational changes in Atg expression status which are also utilized as markers for autophagy. The microtubule-associated protein light chain 3 (LC3B-I) becomes conjugated with phosphatidyl-ethanolamin to form LC3B-II that integrates into the autophagosomal membrane. Atg6/beclin1 is a constituent of the class III PI3 kinase complex that is frequently up-regulated during progression of autophagy. In astrocytes, we observed a well-defined LC3B-I to LC3B-II conversion indicative of autophagosome formation at concentrations of 10 μM AMI and CIT (72 h), while VPA (1, 10 mM), VEN (1, 10 μM, data not shown), and lower doses of AMI/CIT (1 μM) had no effect (Fig. 5A). LC3B-II positive signals were monitored already after 12 h of AMI (10 μM) exposure and steadily increased during 60 h thereafter. The response to 10 μM CIT emerged at a later point in time at 72

h (Fig. 5C). Concomitantly to LC3B-II induction, beclin-1 expression was subtly up-regulated upon treatment with AMI/CIT. In neurons, beclin-1 expression was stable and unchanged after AMI, CIT (both 10 μM, 72 h) and VPA (10 mM, 72 h) application (Fig. 5B). However, we also observed a promotion of LC3B-I conversion in neuronal cultures under the influence of AMI and CIT (10 μM, 72 h), with a time-dependency similar to astrocytic cultures (Fig. 5B, C).

Although classified as functional autophagosomal marker, LC3B-I/II might occasionally be incorporated into protein aggregates when autophagy is blocked (Cieehomska and Tolkovsky 2007; Szeto et al. 2006). Therefore, to corroborate that drug-induced accumulation of lipidated LC3B-II is indeed dependent on enhanced autophagic pathways, we first investigated the effects of AMI in autophagy-deficient mouse embryonic fibroblasts (MEF). These cells are devoid of the gene Atg5, whose product acts in concert with Atg12 on the formation of autophagosomes. Even at the highest concentration of AMI (10 μM, 72 h), there was no increase in LC3B-II, while Atg5 wildtype MEF cells responded with a strong accumulation of LC3B-II to AMI exposure (Fig. 5D). Secondly, we analyzed the distribution of an ectopically expressed GFP-LC3 fusion protein in dependence of AMI exposure (10 μM, 12 h) in primary cortical astrocytes (Fig. 6A, B) and neurons (data not shown). We observed a pronounced punctuate pattern of GFP-LC3 signals after AMI treatment, while the number of GFP-LC3 clusters was by far lower in untreated cells. Thus, all these data indicate that AMI and CIT induce the generation of autophagosomes.

Class III PI3 kinase-dependent pathways contribute to AD-induced autophagic processes - Since class III PI3 kinase-dependent pathways are frequently involved in the generation of autophagosomes, we tested whether they are targeted by ADs. We used the specific pharmacological inhibitor 3-methyladenine (3-MA; 3 mM) and measured the number of GFP-LC3 positive speckles, the amount of AVs as well as the extent of endogenous LC3B-II induction after exposure with AMI or CIT (both 10 μM). We first monitored the redistribution of ectopic GFP-LC3 protein in transiently transfected astrocytes treated with 10 μM AMI alone or in combination with 3 mM 3-MA (both for 12 h). Co-incubation led to a reduction of the number of GFP-LC3 positive speckles as compared to AMI alone (Fig. 6B, C). Astrocytes also responded with a reduced formation of AVs after combined AMI and 3-MA treatment (all for 24 h; 84.35% ± 7.42 compared to AMI alone (set to 100%)) (Fig. 6E). Similar findings were obtained for CIT and 3-MA co-treatment (data not shown). Likewise, in the presence of 3-MA, the induction of endogenous LC3B-II by AMI was attenuated (Fig. 6F). In neurons, the influence of 3-MA on drug-induced formation of AVs as well as LC3B-II was similar to the one in astrocytes (Fig. 6E, F).

Since ADs have been reported to positively affect ROS generation, and ROS positively influence autophagy (Cordero et al. 2009; Scherz-Shouval and Elazar 2007), we also included the radical scavenger vitamin E (150 μM) in this study. Indeed, VitE in combination with 10 μM AMI slightly reduced the quantity of GFP-LC3B-II positive puncta (Fig. 6D), AVs as well as endogenous LC3B-II signals in astrocytes or neurons (Fig. 6E, F). In this context, ROS might facilitate an unfolded protein response of the endoplasmatic reticulum (UPR), which in turn is capable of activating autophagy

(Harding et al. 2003; Hoyer-Hansen and Jaattela 2007). Therefore, we asked whether UPR is triggered due to treatment with AMI or CIT in astrocytes by applying reporter gene assays. The reporter plasmid used contained an Endoplasmatic Reticulum Stress Responsive Element (ERSE) which indicates the up-regulation of transcription factors involved in UPR. Subsequent to transfection, astrocytes were treated with 1 or 10 µM AMI or CIT for 16 h and assayed for luciferase activity. While tunicamycin used as positive control induced a significant up-regulation of reporter gene expression, AMI and CIT did not produce a UPR (Fig. S2).

Together, these data suggest that signaling pathways involving class III PI3 kinase as well as ROS (without UPR contribution) contribute to the extent of drug-induced AV and LC3B-II formation.

Autophagic flux is functional in AMI and CIT exposed astrocytes - Subsequent to autophagosome formation, the cargo-containing vesicles fuse with lysosomes to build autolysosomes, followed by break-down and recycling of their contents. The rate of autophagosome turn-over is also termed autophagic flux. The observed increase in LC3B-II signals could either be due to an enhanced autophagosome production and autophagic flux or a reduced turn-over of autophagosomes. To address this question, we determined LC3B-II levels after AMI treatment in combination with either the proton ATPase inhibitor bafilomycin A (BafA, 20 nM) or the protease inhibitor mix pepstatin A/E-64d (10 µg/ml each). If AMI increases the extent of autophagy, and augments the number of autophagosomes for degradation, a combined treatment with BafA or protease inhibitors should result in a considerable increase of the autophagosomal marker LC3B-

II. After 24 h of AMI co-treatment, BafA indeed led to a marked elevation of LC3B-II levels in astrocytes, while pepstatin A/E-64d produced smaller effects. These effects were not detectable after 12 h suggesting that autophagic flux requires a definite time to be established (Fig. 7A). Again, neurons exhibited a similar response. To corroborate these results, we additionally performed immun-co-localization experiments in order to track LC-3II signals in relation to AVs in astrocytic cells. After 12 h of 10 μM AMI treatment, only a small number of LC-3II immuno-reactive spots were observed in a few cells that mostly did not co-localize with LysoRed. Later, the number of LC3B-II speckles per cell as well as LC3B-II positive cells drastically increased, and to some degree LC3B-II signals overlapped with LysoRed-positive AVs after 72 h (Fig. 7B). In conclusion, these results point to a stimulatory effect of AMI on the production of autophagosomes and subsequent autophagic flux.

Protein – turnover is enhanced in AMI treated astrocytes and neurons – Many species of long-lived proteins are degraded through the autophagic pathway. We therefore addressed the question if the turn-over of long-lived proteins is affected by AMI treatment in neurons and astrocytes. Cells were first treated with 10 μM AMI for a period of 72 h, at which a pulse with ^{3}H-labelled leucine was set in the last 24 h of AMI treatment. After a pre-chase period of 4 h with an excess of cold leucine to deplete radio-labelled short-lived proteins, cells were cultivated for an additional 8 h in medium devoid of AMI, and trichloroacetic acid-soluble and insoluble material was measured from cell lysates and supernatants (Fig. 8A). Trichloroacetic acid-soluble material represented the fraction of degraded proteins. Levels of the LC3B-II marker continued to be elevated,

even 24 and 48 h after wash-out of AMI (Fig. 8B). Increased levels of trichloroacetic acid-soluble components were detected in AMI exposed astrocytes and neurons, suggesting accelerated proteolysis of endogenous long-lived proteins to smaller ^{3}H-containing metabolites (Fig. 8B).

Effects of AMI on mitophagy – Apart from degradation of long-lived proteins, cellular organelles such as dysfunctional mitochondria might also be subjected to autophagy-mediated removal, a phenomenon called mitophagy. Thus, we elucidated the possibility of a globally augmented autophagy-mediated clearance of damaged mitochondria in the course of AMI treatment. First, we determined protein levels of the mitochondria-specific F_0F_1 subunit after 24 h and 72 h of 10 µM AMI treatment. Neither neurons nor astrocytes responded with decreased immuno-reactive signals corresponding to F_0F_1 subunits indicating no significant degradation of mitochondrial organelles (Fig. 9A). At the cellular level, we tracked ectopically expressed GFP-LC3 together with fluorescence-stained mitochondria in astrocytes, and could not detect merging signals under conditions of short-term treatment with 10 µM AMI (24 h) (Fig. 9B, C). Finally, we recorded the localization of mitochondria in relation to lysosomes. After 72 h of AMI (10 µM) treatment, the degree of overlap between MitoTracker Green-stained mitochondria and LysoRed stained AVs was rather small and indistinguishable from control cells (Fig. 9D, E). Hence, mitochondria are no major target of AMI-triggered autophagic processes.

Glial viability is not severely compromised by AMI/CIT-induced autophagy - Autophagy primarily represents an adaptive and cytoprotective process that strives for re-

establishment of physiological cellular states. On the other hand, autophagy might also lead to, or at least coincide with type II cell death when reaching excessive levels or failing to cope with stressful situations. To test for a connection between drug-induced autophagy and cell viability, we determined the effects of the applied drugs on cell viability parameters using either lactate dehydrogenase (LDH) release or MTT assays in case of astrocytes and neurons, respectively (Table 1). Of all ADs tested, the cytotoxic effects of VEN were least prominent in neurons and astrocytes, while AMI and CIT exposure at the highest concentrations (10 μM each, 72 h) caused ~25% increase in LDH release in astrocytes, as compared to 30-45% cell death in neurons as determined by MTT assay. Of all drugs tested, the mood stabilizer VPA exerted the strongest cytotoxic effects.

Following-up the moderately harmful effects of AMI, CIT and VPA at higher concentrations, we intended to define whether type I (caspase-mediated) or type II cell death are attributable. We used two different markers of type-1 cell death, namely cleaved procaspase-3 and DNA fragmentation. Astrocytes were exposed to increasing concentrations of AMI (1-10 μM), CIT (1-10 μM) and VPA (1-10 mM VPA) for 72 h, and cleaved pro-caspase-3 was monitored by Western Blot analysis. Solely 10 mM VPA exposure led to a subtle induction of pro-caspase-3 cleavage, whereas AMI and CIT did not exert any effect. Co-incubation of AMI or CIT with VPA produced marked caspase-3 activation (Fig. 10). Accordingly, DNA fragmentation was not present in cells exposed to AMI or CIT as determined by TUNEL assay (data not shown). Unlike astrocytes, neurons reacted with a pronounced induction of pro-caspase-3 cleavage in response to VPA (10 mM), and to a smaller extent to AMI (10 μM) and CIT (10 μM). VPA treatment

provoked the fastest response, while pro-caspase-3-cleavage emerged within a time span of 72 h in the case of AMI and CIT application (Fig. 10). Drug-treated neurons also displayed a number of nuclei containing fragmented DNA as evidenced by TUNEL staining, and the extent of fragmentation clearly correlated with the intensity of pro-caspase-3 cleavage (data not shown).

Discussion

In the present study, we show for the first time that the antidepressants AMI and CIT stimulated autophagic processes in astrocytes and neurons. VEN and VPA did not elicit signs of increased autophagy in either cell type. Applied at higher concentrations, AMI/CIT evoked major features of autophagy including up-regulation of LC3B-II and enhanced proteolysis of long-lived proteins. The autophagic flux appeared to be unhampered after AMI treatment, even though free cholesterol accumulated in AV/lysosomal compartments. AMI partially acted through class III PI3 kinase (Vps34) and ROS-dependent signaling pathways, since 3-MA and VitE diminished the effects of AMI-induced autophagic marker production. The enzymatic activity of Vps34 is regulated by an orchestrated action of Vps15, beclin1 and UVRAG that are all found at nearly stoichiometric levels in a core complex with Vps34 (Zhong et al. 2009). Thus, AMI impacts on autophagy via a central complex that governs the nucleation of autophagic vesicles and therefore participates in the central step of autophagy initiation.

Recent studies derived from NP-C disease models suggested that distinct physiological states such as altered cholesterol trafficking might also promote autophagy (Liao et al. 2007; Pacheco et al. 2007). NP-C disorder is characterized by disturbances in lipid and cholesterol shuttling and by elevated levels of autophagic markers. Analysis of NP-C derived fibroblasts revealed a ~10-fold increase of intracellular cholesterol pools mainly localized in AVs yet unchanged membrane cholesterol levels as compared to normal fibroblasts (Lange et al. 2000). The lysosomal influx of cholesterol is considered to be abnormally high which is ascribed to non-functional NPC proteins. Since NP-C disease features many aberrant intracellular events, it is challenging to decipher potential attributions of altered cholesterol homeostasis and vacuolization to activated autophagic pathways.

Interestingly, treatment of fibroblasts with amphiphilic substances mimics certain aspects of the NP-C phenotype including vacuolization, a substantial rise in cytoplasmic cholesterol content and its redistribution into AVs (Anderson and Borlak 2006). Cationic amphiphilic drugs (CADs) including AMI, CIT and VEN belong to a class of compounds consisting of a hydrophobic ring structure and a side chain with a charged cationic amine group. Also AMI and CIT induced the formation of cholesterol-loaded AVs, but only AMI positively affected cholesterol synthesis ultimately leading to slightly increased cytoplasmic cholesterol levels which were not reflected in total cell cholesterol content. Similarly, treatment of C6 glioma cells with desipramine did not change total cholesterol levels (Donati and Rasenick 2005). The slight increase of cholesterol biosynthesis observed in AMI-treated cells might take place in order to compensate for lysosomally captured cholesterol. The extent of change in cytoplasmic cholesterol levels was

magnitudes lower compared to NP-C derived fibroblasts or class I amphiphile (U18666A) treated cells (Lange et al. 2000). In parallel to AMI-induced elevated cytoplasmic cholesterol concentrations, the cholesterol trafficking gene NPC2 was up-regulated indicating that the respective regulatory mechanism of cholesterol shuttling is not fundamentally disturbed. Similar effects of ADs on HMG-CoA reductase and NPC2 regulation are known for cell lines (Raeder et al. 2006b; Vik-Mo et al. 2010). From our data we conclude that AV formation and concomitant cholesterol sequestration does not depend on augmented cholesterol biosynthesis or aberrant expression of NPC as reported for NP-C disorder. It might be rather related to the biophysical properties of AMI and CIT acting as CADs on processes related to lysosomal lipid/cholesterol aggregation. Lysosomal structures in turn might facilitate autophagy induction. Altogether, a multitude of biophysical and biochemical modes of action of AMI and CIT seem to route the chronological progress of vacuole formation and autophagy in a dose-dependent fashion. The CAD VEN neither induced vacuolization nor autophagy, implying that additional factors determine the outcome on vesicle formation and autophagy.

Autophagy-modulating compounds are considered to be promising future therapeutics for the treatment of cancer and neuropsychiatric disorders. Up to date, a number of exogenous factors have been identified that influence autophagy with a remarkable variety of modes of action as well as cell type specificity. Among the group of regulators are rapamycin, cadmium ions, valproic acid, lithium and fluoxetin. Rapamycin represents a ubiquitous inducer of autophagy since it inhibits mTOR kinases. The mTOR kinase is a key switch to keep autophagic pathways operating at low levels, where inhibition of

mTOR results in the release of positive regulators of autophagy (Shigemitsu et al. 1999). Cadmium ions act independently of mTOR via elevation of cytoplasmic calcium stemming from the endoplasmic reticulum and subsequent ERK1/2 activation in mesangial cell lines (Wang et al. 2008). The mood-stabilizing and anticonvulsive drug VPA has lately been demonstrated to stimulate ERK1/2 phosphorylation in concert with ROS thereby promoting autophagy in human glioma cells (Fu et al. 2010). Lithium salts are also widely prescribed mood-stabilizers, yet use another molecular mechanism, since they interfere with the cellular myo-inositol homeostasis by blocking inositol monophosphatases (Sarkar et al. 2005). Lately, maprotiline and fluoxetin were reported to increase LC3B-II levels in lymphoma derived cell lines although no evidence for an operative mode of autophagy was provided (Cloonan and Williams 2010).

Cancer cells occasionally use autophagy to resist the cytotoxic impact of chemotherapeutics (Dalby et al. 2010). Thus, transformed cells are more susceptible to chemotherapeutics when autophagy is pharmacologically inhibited. For instance, co-treatment of HeLa cells with desmethyl-clomipramine, which blocks autophagy, and the DNA-damaging agent doxorubicin results in potentiation of the cytotoxic effects of doxorubicin (Rossi et al. 2009).

In the central nervous system, both protective and detrimental functions have been ascribed to autophagy, and disentangling causative relations is still an unresolved issue. During early development, autophagic processes provide energy by means of ATP generated from recycled amino acids fed into the tricarboxylic cycle. ATP in turn delivers energy for the removal of apoptotic cells through engulfment and subsequent degradation. In the mature CNS, mechanical or biochemical insults of neurons are often

accompanied by autophagy which is thought to promote regenerative events or cell destruction, depending on the spatial-temporal context (Boya et al. 2008).

Here, we demonstrated marked differences in the type of cell death between neurons and astrocytes after drug application. Apoptotic cell death was absent in astrocytes which nevertheless showed signs of moderately diminished cell viability after exposure to 10 μM AMI or CIT. We speculate that enhanced autophagy including slightly increased beclin1 protein levels in astrocytes might confer some resistance against apoptotic signals. Still, autophagy does not accomplish cellular recovery from AMI- or CIT-mediated toxicity, and thus, the question remains whether autophagy accounts for or coincides with cell death which simply may be a consequence of extensive vacuolization or aggregation of lipids/cholesterol. Therefore, we can not exclude that autophagy may even implement a back-up system for removing irreversibly damaged astroglial cells, under conditions where apoptosis is not efficiently conducted.

Neurons underwent type I caspase-dependent cell death in response to higher doses of AMI/CIT (10 μM). Interestingly, autophagy was initiated roughly 2 days before the onset of apoptosis and therefore is unlikely to account directly for activated caspase-3 and DNA fragmentation. Numerous studies describe apoptotic events arising from AD exposure, employing either glioma cell lines, fibroblasts or dorsal root ganglia neurons as cellular models (Levkovitz et al. 2005; Lirk et al. 2006; Moreno-Fernandez et al. 2008).

The use of autophagy modulators in CNS tissue may comprise neurodegenerative and psychiatric conditions. Many aggregate-prone proteins are substrates of autophagy and can be effectively cleared from the cytosol after autophagy induction. For instance, lithium salts were reported to mediate the reduction of mutant huntingtin and α-

synucleins in neuronal precursor cell lines and COS-7 cells (Sarkar et al. 2005). Since both, AMI and CIT showed moderate increases in the expression of autophagic markers paralleled by enhanced protein turnover, we suggest that these compounds could represent potential candidates controlling the turn-over of aggregate-prone proteins in neurodegenerative disorders. Of note, rapamycin exerts antidepressive-like effects in animal models suggesting that autophagy might not solely be a promising target for treatment of neurodegenerative, but also psychiatric conditions (Cleary et al. 2008b; Cleary et al. 2008a). Apart from an imbalance of the neurotransmitter homeostasis, aberrant metabolic as well as immune-related functions are thought to contribute to the pathogenesis of affective disorders. A hypothetical deficit of energy as indicated by reduced levels of ATP and creatine phosphate in the brain of many patients (Moretti et al. 2003) as well as an over-reactive immune system as mirrored by increases in cytokine levels are features that occur during disease manifestation (Penninx et al. 2003; Thomas et al. 2005). Here, drug-induced autophagy might serve several functions: first, energy metabolism might be partly reconstituted by enhanced proteolysis and subsequent generation of ATP. Lending support to this hypothesis, amitriptyline-treated astrocytes show increased levels of ATP (Trzeciak et al. 1995). Second, AD-induced autophagy might dampen the production and release of certain interleukins, interferons and reactive oxygen species and thereby bring about anti-inflammatory actions (Rouschop KM et al. 2009; Saitoh et al. 2008).

In conclusion, the diverse effects of three widely described ADs on autophagy support the view that these drugs can be differentiated according to their impact beyond monoaminergic neurotransmission. It is tempting to speculate that AD-mediated

autophagy might help to restore certain metabolic and immunological pathways (Fig. 11). Albeit autophagy exhibits a variety of reported beneficial properties, further studies need to assess and carefully balance the risk of potential harmful side effects in the CNS.

Disclosure/Conflict of Interest

None

Acknowledgements

We appreciate the excellent technical assistance of K. Hafner, and are grateful to T. Yoshimori for providing the rat pEGFP-LC3 expression vector, K. Winkelhofer for luciferase reporter vectors and N. Mizushima for generously providing Atg5 depleted MEF cells. This study was supported in part by the Max Planck Society and NARSAD Young Investigator Award (to J.Z.).

Supplementary information is available at the *Neuropsychopharmacology* website**.**

Reference List

Alakoskela JM, Vitovic P, Kinnunen PKJ (2009). Screening for the Drug-Phospholipid Interaction: Correlation to Phospholipidosis. *Chemmedchem* **4**: 1224-1251.

Anderson N, Borlak J (2006). Drug-induced phospholipidosis. *Febs Letters* **580**: 5533-5540.

Bayatti N, Zschocke J, Behl C (2003). Brain region-specific neuroprotective action and signaling of corticotropin-releasing hormone in primary neurons. *Endocrinology* **144**: 4051-4060.

Berridge MV, Tan AS (1993). Characterization of the Cellular Reduction of 3-(4,5-Dimethylthiazol-2-Yl)-2,5-Diphenyltetrazolium Bromide (Mtt) - Subcellular-Localization, Substrate Dependence, and Involvement of Mitochondrial Electron-Transport in Mtt Reduction. *Archives of Biochemistry and Biophysics* **303**: 474-482.

Bouman L, Schlierf A, Lutz AK, Deinlein A, Shan J, Kast J*, et al.* (2010): Parkin is transcriptionally regulated by ATF4: evidence for an interconnection between mitochondrial stress and ER stress. In press. Cell Death and Differentiation.

Boya P, Mellen MA, de la Rosa EJ (2008). How autophagy is related to programmed cell death during the development of the nervous system. *Biochemical Society Transactions* **36**: 813-817.

Carvalho LA, Garner BA, Dew T, Fazakerley H, Pariante CM (2010). Antidepressants, but not antipsychotics, modulate GR function in human whole blood: An insight into molecular mechanisms. *European Neuropsychopharmacology* **20**: 379-387.

Chang TY, Reid PC, Sugii S, Ohgami N, Cruz JC, Chang CCY (2005). Niemann-Pick type C disease and intracellular cholesterol trafficking. *Journal of Biological Chemistry* **280**: 20917-20920.

Cieehomska IA, Tolkovsky AM (2007). Non-autophagic GFP-LC3 puncta induced by saponin and other detergents. *Autophagy* **3**: 586-590.

Cleary C, Hadas I, Belmaker HR, Agam G, Flaisher-Grinberg S, Einat H (2008a). Antidepressant-like effects of the mTOR inhibitor rapamycin: Further behavioral and biochemical evidence. *Biological Psychiatry* **63**: 101S-102S.

Cleary C, Linde JAS, Hiscock KM, Hadas I, Belmaker RH, Agam G*, et al.* (2008b). Antidepressive-like effects of rapamycin in animal models: Implications for mTOR inhibition as a new target for treatment of affective disorders. *Brain Research Bulletin* **76**: 469-473.

Cloonan SM, Williams D.V. (2010): The antidepressants maprotiline and fluoxetine induce Type II autophagic cell death in drug-resistant Burkitt's lymphoma. In. International Journal of Cancer.

Corcelle EA, Puustinen P, Jaattela M (2009). Apoptosis and autophagy: Targeting autophagy signalling in cancer cells -'trick or treats'? *Febs Journal* **276**: 6084-6096.

Cordero MD, Moreno-Fernandez AM, Gomez-Skarmeta JL, de Miguel M, Garrido-Maraver J, Oropesa-Avila M*, et al.* (2009). Coenzyme Q(10) and alpha-tocopherol protect against amitriptyline toxicity. *Toxicology and Applied Pharmacology* **235**: 329-337.

Czeh B, Simon M, Schmelting B, Hiemke C, Fuchs E (2006). Astroglial plasticity in the hippocampus is affected by chronic psychosocial stress and concomitant Fluoxetine treatment. *Neuropsychopharmacology* **31**: 1616-1626.

Dalby KN, Tekedereli I, Lopez-Berestein G, Ozpolat B (2010). Targeting the prodeath and prosurvival functions of autophagy as novel therapeutic strategies in cancer. *Autophagy* **6**: 322-329.

Donati RJ, Rasenick MM (2005). Chronic antidepressant treatment prevents accumulation of Gs alpha in cholesterol-rich, cytoskeletal-associated, plasma membrane domains (lipid rafts). *Neuropsychopharmacology* **30**: 1238-1245.

Donati RJ, Thukral C, Rasenick MM (2001). Chronic treatment of C6 glioma cells with antidepressant drugs results in a redistribution of Gs alpha. *Molecular Pharmacology* **59**: 1426-1432.

Franke B, Figiel M, Engele J (1998). CNS glia are targets for GDNF and neurturin. *Histochemistry and Cell Biology* **110**: 595-601.

Fu J, Shao CJ, Chen FR, Ng HK, Chen ZP (2010). Autophagy induced by valproic acid is associated with oxidative stress in glioma cell lines. *Neuro-Oncology* **12**: 328-340.

Glick D, Barth S, Macleod KF (2010). Autophagy: cellular and molecular mechanisms. *Journal of Pathology* **221**: 3-12.

Glotzbach RK, Preskorn SH (1982). Brain Concentrations of Tricyclic Anti-Depressants - Single-Dose Kinetics and Relationship to Plasma-Concentrations in Chronically Dosed Rats. *Psychopharmacology* **78**: 25-27.

Gozuacik D, Kimchi A (2004). Autophagy as a cell death and tumor suppressor mechanism. *Oncogene* **23**: 2891-2906.

Harding HP, Zhang YH, Zeng HQ, Novoa I, Lu PD, Calfon M*, et al.* (2003). An integrated stress response regulates amino acid metabolism and resistance to oxidative stress. *Molecular Cell* **11**: 619-633.

Herr AS, Tsolakidou AF, Yassouridis A, Holsboer F, Rein T (2003). Antidepressants differentially influence the transcriptional activity of the glucocorticoid receptor in vitro. *Neuroendocrinology* **78**: 12-22.

Hisaoka K, Takebayashi M, Tsuchioka M, Maeda N, Nakata Y, Yamawaki S (2007). Antidepressants increase glial cell line-derived neurotrophic factor production through monoamine-independent activation of protein tyrosine kinase and extracellular signal-regulated kinase in glial cells. *Journal of Pharmacology and Experimental Therapeutics* **321**: 148-157.

Holladay JW, Dewey MJ, Yoo SD (1998). Pharmacokinetics and antidepressant activity of fluoxetine in transgenic mice with elevated serum alpha-1-acid glycoprotein levels. *Drug Metabolism and Disposition* **26**: 20-24.

Hoyer-Hansen M, Jaattela M (2007). Connecting endoplasmic reticulum stress to autophagy by unfolded protein response and calcium. *Cell Death and Differentiation* **14**: 1576-1582.

Huang WP, Klionsky DJ (2002). Autophagy in yeast: A review of the molecular machinery. *Cell Structure and Function* **27**: 409-420.

Kuma A, Hatano M, Matsui M, Yamamoto A, Nakaya H, Yoshimori T*, et al.* (2004). The role of autophagy during the early neonatal starvation period. *Nature* **432**: 1032-1036.

Lange Y, Ye J, Rigney R, Steck T (2000). Cholesterol movement in Niemann-Pick type C cells and in cells treated with amphiphiles. *Journal of Biological Chemistry* **275**: 17468-17475.

Levkovitz Y, Gil-Ad I, Zeldich E, Dayag M, Weizman A (2005). Differential induction of apoptosis by antidepressants in glioma and neuroblastoma cell lines - Evidence for p-c-Jun, cytochrome c, and caspase-3 involvement. *Journal of Molecular Neuroscience* **27**: 29-42.

Liao G, Yao Y, Liu J, Cheung S, Xie A (2007). Autophagic-lysosomal dysfunction is associated with cholesterol accumulation and neurodegeneration in NPC1-/- mice. *Journal of Neurochemistry* **102**: 36.

Lirk P, Haller I, Hausott B, Ingorokva S, Deibl M, Gerner P*, et al.* (2006). The neurotoxic effects of amitriptyline are mediated by apoptosis and are effectively blocked by inhibition of caspase activity. *Anesthesia and Analgesia* **102**: 1728-1733.

Liu YB, Peterson DA, Kimura H, Schubert D (1997). Mechanism of cellular 3-(4,5-dimethylthiazol-2-yl)-2,5-diphenyltetrazolium bromide (MTT) reduction. *Journal of Neurochemistry* **69**: 581-593.

Livak KJ, Schmittgen TD (2001). Analysis of relative gene expression data using real-time quantitative PCR and the 2(T)(-Delta Delta C) method. *Methods* **25**: 402-408.

Mehrpour M, Esclatine A, Beau I, Codogno P (2010). Autophagy in health and disease. 1. Regulation and significance of autophagy: an overview. *American Journal of Physiology-Cell Physiology* **298**: C776-C785.

Moosmann B, Skutella T, Beyer K, Behl C (2001). Protective activity of aromatic amines and imines against oxidative nerve cell death. *Biological Chemistry* **382**: 1601-1612.

Moreno-Fernandez AM, Cordero MD, de Miguel M, gado-Rufino MD, Sanchez-Alcazar JA, Navas P (2008). Cytotoxic effects of amitriptyline in human fibroblasts. *Toxicology* **243**: 51-58.

Moretti A, Gorini A, Villa RF (2003). Affective disorders, antidepressant drugs and brain metabolism. *Molecular Psychiatry* **8**: 773-785.

Nothdurfter C, Tanasic S, Di Benedetto B, Rammes G, Wagner EM, Kirmeier T*, et al.* (2010). Impact of Lipid Raft Integrity on 5-HT3 Receptor Function and its Modulation by Antidepressants. *Neuropsychopharmacology* **35**: 1510-1519.

Owens MJ, Morgan WN, Plott SJ, Nemeroff CB (1997). Neurotransmitter receptor and transporter binding profile of antidepressants and their metabolites. *Journal of Pharmacology and Experimental Therapeutics* **283**: 1305-1322.

Pacheco CD, Kunkel R, Lieberman AP (2007). Autophagy in Niemann-Pick C disease is dependent upon Beclin-1 and responsive to lipid trafficking defects. *Human Molecular Genetics* **16**: 1495-1503.

Paez-Pereda M (2005). New drug targets in the signaling pathways activated by antidepressants. *Progress in Neuro-Psychopharmacology & Biological Psychiatry* **29**: 1010-1016.

Penninx BWJH, Kritchevsky SB, Yaffe K, Newman AB, Simonsick EM, Rubin S*, et al.* (2003). Inflammatory markers and depressed mood in older persons: Results from the Health, Aging and Body Composition study. *Biological Psychiatry* **54**: 566-572.

Perisic T, Zimmermann N, Kirmeier T, Asmus M, Tuorto F, Uhr M*, et al.* (2010). Valproate and Amitriptyline Exert Common and Divergent Influences on Global and Gene Promoter-Specific Chromatin Modifications in Rat Primary Astrocytes. *Neuropsychopharmacology* **35**: 792-805.

Raeder MB, Bjelland I, Ferno J, Vollset SE, Steen VM (2006a). Lipogenic effects of antidepressant drugs: Transcriptional stimulation of cellular lipid biosynthesis is a potential marker of drug-induced metabolic side-effects. *Nordic Journal of Psychiatry* **60**: 336.

Raeder MB, Ferno J, Glambek M, Stansberg C, Steen VM (2006b). Antidepressant drugs activate SREBP and up-regulate cholesterol and fatty acid biosynthesis in human glial cells. *Neuroscience Letters* **395**: 185-190.

Rodriguez-Lafrasse C, Rousson R, Bonnet J, Pentchev PG, Louisot P, Vanier MT (1990). Abnormal Cholesterol-Metabolism in Imipramine-Treated Fibroblast-Cultures - Similarities with Niemann-Pick Type-C Disease. *Biochimica et Biophysica Acta* **1043**: 123-128.

Rossi M, Munarriz ER, Bartesaghi S, Milanese M, Dinsdale D, Guerra-Martin MA*, et al.* (2009). Desmethylclomipramine induces the accumulation of autophagy markers by blocking autophagic flux. *Journal of Cell Science* **122**: 3330-3339.

Rouschop KM, Ramaekers CH, Schaaf MB, Keulers TG, Savelkouls KG, Lambin P*, et al.* (2009): Autophagy is required during cycling hypoxia to lower production of reactive oxygen species. *Radiother Oncol* **92**: 411-416.

Saitoh T, Fujita N, Jang MH, Uematsu S, Yang BG, Satoh T*, et al.* (2008). Loss of the autophagy protein Atg16L1 enhances endotoxin-induced IL-1 beta production. *Nature* **456**: 264-U68.

Sarkar S, Floto RA, Berger Z, Imarisio S, Cordenier A, Pasco M*, et al.* (2005). Lithium induces autophagy by inhibiting inositol monophosphatase. *Journal of Cell Biology* **170**: 1101-1111.

Scherz-Shouval R, Elazar Z (2007). ROS, mitochondria and the regulation of autophagy. *Trends in Cell Biology* **17**: 422-427.

Schulke JP, Wochnik GM, Lang-Rollin I, Gassen NC, Knapp RT, Berning B*, et al.* (2010). Differential Impact of Tetratricopeptide Repeat Proteins on the Steroid Hormone Receptors. *Plos One* **5**.

Shigemitsu K, Tsujishita Y, Hara K, Nanahoshi M, Avruch J, Yonezawa K (1999). Regulation of translational effectors by amino acid and mammalian target of rapamycin signaling pathways - Possible involvement of autophagy in cultured hepatoma cells. *Journal of Biological Chemistry* **274**: 1058-1065.

Shimizu S, Kanaseki T, Mizushima N, Mizuta T, rakawa-Kobayashi S, Thompson CB*, et al.* (2004). Role of Bcl-2 family proteins in a non-apoptotic programmed cell death dependent on autophagy genes. *Nature Cell Biology* **6**: 1221-1228.

Szeto J, Kaniuk NA, Canadien V, Nisman R, Mizushima N, Yoshimori T*, et al.* (2006). ALIS are stress-induced protein storage compartments for substrates of the proteasome and autophagy. *Autophagy* **2**: 189-199.

Thomas AJ, Davis S, Morris C, Jackson E, Harrison R, O'Brien JT (2005). Increase in interleukin-1 beta in late-life depression. *American Journal of Psychiatry* **162**: 175-177.

Trzeciak HI, Kalacinski W, Malecki A, Kokot D (1995). Effect of Neuroleptics on Phospholipase A(2) Activity in the Brain of Rats. *European Archives of Psychiatry and Clinical Neuroscience* **245**: 179-182.

Vik-Mo AO, Fernø J., Skrede S., Steen VM. (2009): Psychotropic drugs up-regulate the expression of cholesterol transport proteins including ApoE in cultured human CNS- and liver cells. *BMC Pharmacology* **9:10**

Wang SH, Shih YL, Ko WC, Wei YH, Shih CM (2008). Cadmium-induced autophagy and apoptosis are mediated by a calcium signaling pathway. *Cellular and Molecular Life Sciences* **65**: 3640-3652.

Xia ZL, Ying G, Hansson AL, Karlsson H, Xie Y, Bergstrand A*, et al.* (2000). Antidepressant-induced lipidosis with special reference to tricyclic compounds. *Progress in Neurobiology* **60**: 501-512.

Xu Z, Farver W, Kodukula S, Storch J (2008). Regulation of sterol transport between membranes and NPC2. *Biochemistry* **47**: 11134-11143.

Zhong Y, Wang QJ, Li XT, Yan Y, Backer JM, Chait BT*, et al.* (2009). Distinct regulation of autophagic activity by Atg14L and Rubicon associated with Beclin 1-phosphatidylinositol-3-kinase complex. *Nature Cell Biology* **11**: 468-U262.

Titles and Legends to Figures

Figure 1 Antidepressants diversely induce formation of cytoplasmic vacuolic structures in primary astrocytes and neurons. Fluorescence images of AMI, CIT and VEN (all 10 μM, 72 h) as well as VPA (10 mM, 72 h) exposed astrocytes and neurons. AVs were visualized by LysoRed staining (red). Identity of cells was validated by immuno-cytochemistry using glial fibrillary acidic protein ($GFAP^+$) and microtubule-associated protein 2 ($MAP2^+$) specific (green) as marker for glial and neuronal origin. Cell nuclei were counterstained with DAPI (blue).

Figure 2 Free cholesterol accumulates in AVs of astrocytes. A) Astrocytes were treated with AMI or CIT (each at 10 μM, 72 h), and free cholesterol was visualized using filipin dye. **B)** Overlay of LysoRed and filipin derived fluorescence signals reveals co-localization of AVs and free cholesterol in AMI and CIT treated astrocytes.

Figure 3 Quantification of AVs demonstrates a dose- and time-dependent increase in response to ADs. A) Various concentrations of AMI and CIT ranging from 0.1 – 10 μM were applied to cortical astrocytes for 72 h and the generation of AVs was determined by staining with LysoRed. CellTracker Green signal was used for normalization on cell number and volume. Control has been set to 1 (mean ± SD, n = 3, *$p \leq 0.05$). **B)** Time course (12 h – 72 h) of 10 μM AMI and CIT exposure of cortical astrocytes and subsequent relative LysoRed quantification (control set to 1). **C)**

Comparison of AV production in astrocytes (black bars) and neurons (grey bars). Cells were treated with AMI, CIT, VEN and VPA at the indicated concentrations for 72 h. Graph depicts fold increase in LysoRed signal compared to untreated control (set to 1).

Figure 4 Effects of AMI/CIT on neural cholesterol homeostasis. A, B) Expression analysis of HMG-CoA reductase (A) and NPC2 mRNA (B) levels in astrocytes and neurons that were incubated with either 10 μM AMI or CIT for the indicated time periods. Real time PCR quantification of HMG-CoA reductase and NPC2 mRNA levels was normalized to the respective levels of actin (n=3, mean ± SD, *$p \leq 0.05$ vs. control). **C, D)** AMI evokes cytoplasmic rise in free cholesterol (C), but leaves total cholesterol unaffected (D). Total and cytoplasmic extracts were prepared from cortical astrocytes treated with 10 μM AMI or CIT for 72 h. Data are depicted as μg of free cholesterol per 1 mg of protein (n=3, mean ± SD, *$p \leq 0.05$ vs. control). In addition, cholesterol concentrations in total extracts of drug-exposed neurons were also determined using AmplexRed (D).

Figure 5 Effects of psycho-active drugs on autophagic markers LC3B-II and beclin1 A, B) Extracts of astrocytes (A) and neurons (B) exposed to AMI, CIT and VPA at the indicated concentrations were subjected to Western blot for analysis of LC3B-I/II and beclin1. Actin immuno-reactivity served as loading control. **C)** Time course of LC3B-II induction upon treatment with AMI and CIT. **D)** Treatment of wildtype and Atg5 knockout MEF cells with AMI at the specified concentrations and times reveals dependency of LC3B-II induction on Atg5.

Figure 6 AMI impacts on ectopically expressed GFP-LC3 – contribution of the class III PI3 kinase pathway and ROS. A-D) Astrocytes (~ 2 x 10^6) were transfected with 5 µg of EGFP-LC3 expression plasmid and allowed to recover for 24 h. Horse serum containing medium was changed to MEM/F12/N2 and treatment was started for 12 h with 10 µM AMI alone (B) or in combination with 3 mM 3-MA (C) or 150 µM VitE (D). **E, F)** Astrocytes and neurons were treated with 10 µM AMI together with either 3 mM 3-MA or 150 µM VitE for 24 h. **E)** Cells were incubated for 30 min with LysoRed and CellTracker green dye and dissociated by trypsinization for determination of fluorescence intensities. Corrected LysoRed intensity has been set to 100% in case of AMI treatment without (w/o) inhibitors (mean ± SD, n=3, *$p \leq 0.05$ vs. control). **F)** Lysates of treated and untreated astrocytes and neurons were probed for endogenous LC3B-I/II protein levels by applying Western blot analysis.

Figure 7 Autophagosome turnover is not affected by AMI in cortical astrocytes. A) Astrocytes and neurons were treated with 10 µM AMI for the indicated time periods combined with the ATPase inhibitor BafA (20 nM) or the protease inhibitor mix E-64d/pepstatin A (10 µg/ml each). Cellular lysates were analyzed by Western blot using antibodies directed against LC3B. **B)** Subsequent to exposure to AMI (10 µM; 12 h and 72 h), astrocytes were first stained *in vivo* with LysoRed dye for 30 min, and eventually subjected to immuno-cytochemistry using a LC3B specific primary antibody and Cy2-coupled secondary antibody. DAPI dye served to counterstain cell nuclei.

Figure 8 AMI enhances turn-over of long-lived proteins. A) Scheme depicts treatment regime and ^{3}H-leucine-labeling procedure including pre-chase *(a)* and chase *(b)* periods for astrocytes and neurons. **B)** After 4 h of pre-chase and 8 h of chase period, supernatants and cell lysates were collected and separated into trichloroacetic acid-soluble and insoluble fractions. After determination of cpm values, ratios of trichloroacetic acid soluble vs. insoluble fractions were calculated (mean ± SD, n=2, *$p \leq 0.05$ vs. control). Western blot analysis of cellular extracts derived from astrocytes and neurons previously treated with AMI (10 µM, 72 h) followed by an either 24 h or 48 h wash-out period, or without wash-out (w/o), proofed maintained expression of the autophagy marker LC3B-II also in the absence of the stimulus.

Figure 9 Mitochondria are no substrates for AMI-induced autophagy. A) Astrocytes and neurons were treated as indicated and extracts were probed with antibodies directed against the F_0F_1 subunit of the mitochondrial ATPase complex. Actin immuno-detection was used as control for protein loading. **B, C)** Astrocytes were transfected with pEGFP-LC3, and 24 h post-transfection, cells were treated with 10 µM AMI (24 h) and stained in parallel with Mitotracker Red. After completion of AMI treatment, cells were fixed, nuclei were stained with DAPI, and visualized using confocal microscopy. **D, E)** Astrocytes treated with 10 µM AMI for 72 h were subsequently stained for AVs (LysoRed) as well as for mitochondria (MitoGreen).

Figure 10 Neurons exhibit activated caspase-3 response as result of drug application. Astrocytes and neurons were treated as indicated, and lysates were probed

for cleaved caspase-3. Co-treatments were with AMI and VPA or CIT and VPA at specified concentrations. Actin and Hsc70-specific antibodies served to ensure equal protein loading.

Figure 11 Model of autophagy- and cholesterol-related effects of AMI on astrocytes. AMI triggers autophagic pathways partly via PI3 kinase III- and ROS-dependent signaling that results in enhanced proteolysis. This process comes along with increased levels of beclin1, LC3B-II and lysosomal vesicles. Alterations of HMG-CoA reductase mRNA and cytoplasmic cholesterol levels seem not to be directly linked to autophagy induction but rather to represent accompanying factors. Autophagy can serve several functions: it delivers energy and under certain conditions negatively influences the generation of factors promoting inflammation such as ROS. Thereby, it might support beneficial effects of AMI action apart from monoaminergic neurotransmission. On the other hand, it might contribute to compromised cell integrity as measured by LDH release. *(AP autophagosome, AV acidic vacuoles, AL autophagolysosome)*

Tables

Table 1 Evaluation of neuronal and astroglial viability after drug exposure

	VPA [mM]		
	1	5	10
Astro.	74.42 ± 9.44[a]	59.92 ± 7.21[a]	49.62 ± 11.58[a]
Neuron	82.35 ± 18.49[a]	80.25 ± 10.70[a]	56.40 ± 6.43 [a]

	AMI [µM]	
1	5	10
80.53 ± 10.09[b]	76.41 ± 10.67[b]	73.94 ± 7.66[b]
89.31 ± 7.87 [a]	74.42 ± 8.03[a]	55.37 ± 0.52[a]

	CIT [mM]		
	1	5	10
Astro.	88.09 ± 5.62[b]	89.86 ± 10.75[b]	78.22 ± 5.50[b]
Neuron	98.63 ± 15.38[a]	86.48 ± 4.38[a]	71.11 ± 16.11[a]

	VEN [µM]	
1	5	10
98.02 ± 9.29 [a]	92.87 ± 9.06[a]	87.1 ± 11,45[a]
97.33 ± 9.38 [a]	102.84 ± 3.28 [a]	101.8 ± 4.0[a]

Primary astrocytes and neurons were treated with indicated substances for 72 h. Values are percent of cell viability as compared to untreated control (set to 100%);

[a)] MTT assay; [b)] LDH release assay.

Figure 1

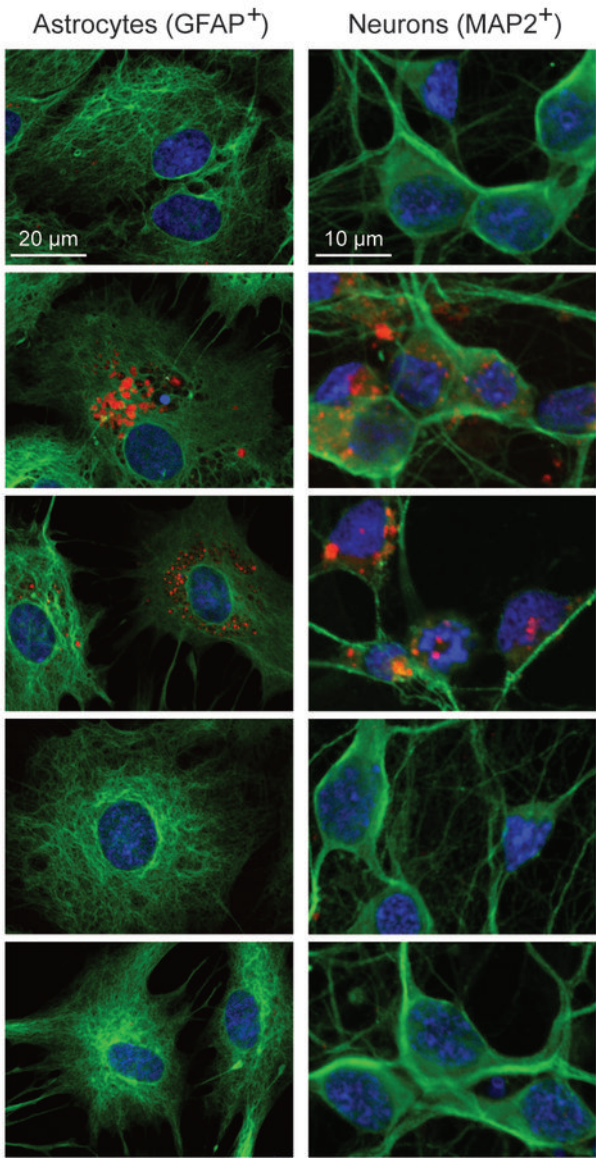
Astrocytes (GFAP+)
Neurons (MAP2+)
Control
10 µM AMI
10 µM CIT
10 µM VEN
10 mM VPA
20 µm
10 µm

Figure 2

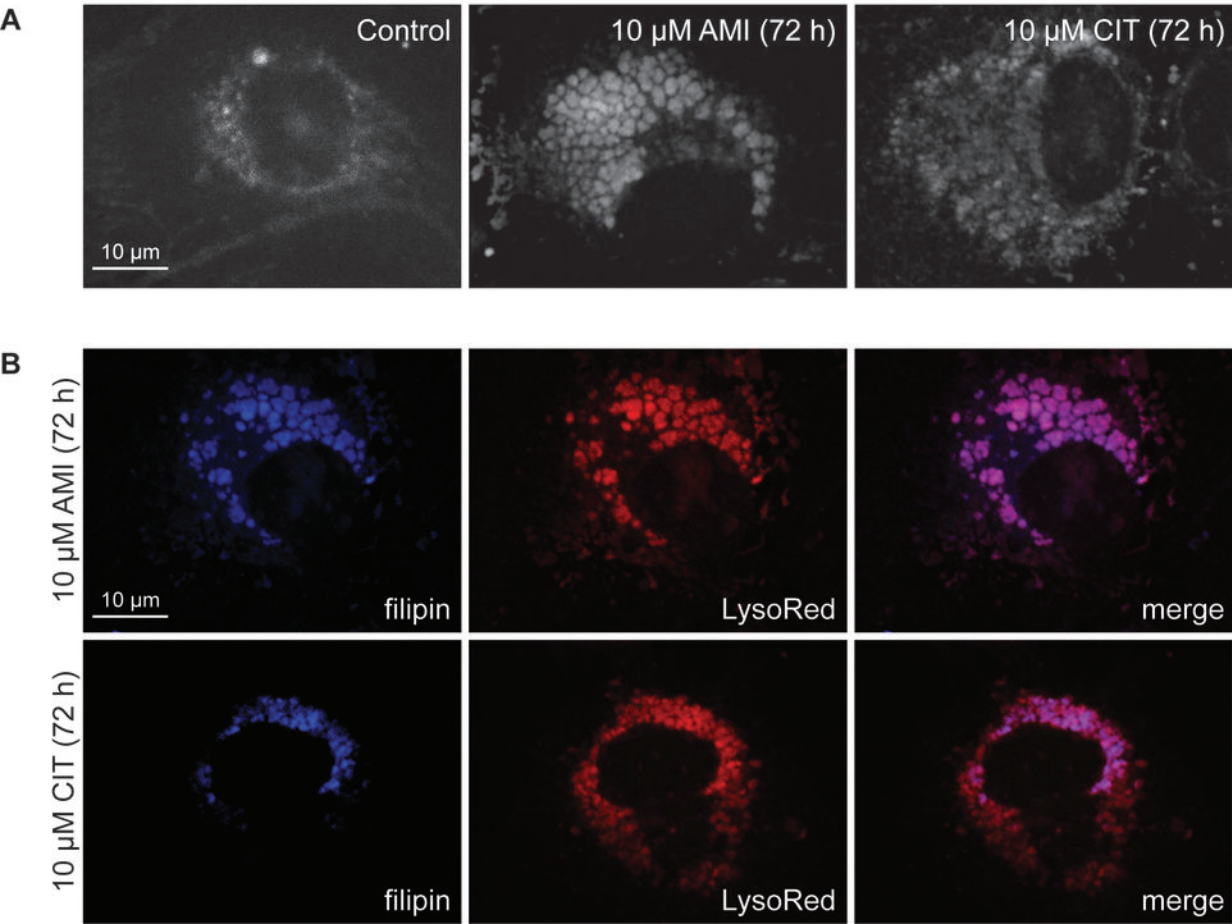
A
Control
10 µM AMI (72 h)
10 µM CIT (72 h)
10 µm
B
10 µM AMI (72 h)
10 µm
filipin
LysoRed
merge
10 µM CIT (72 h)
filipin
LysoRed
merge

Figure 3

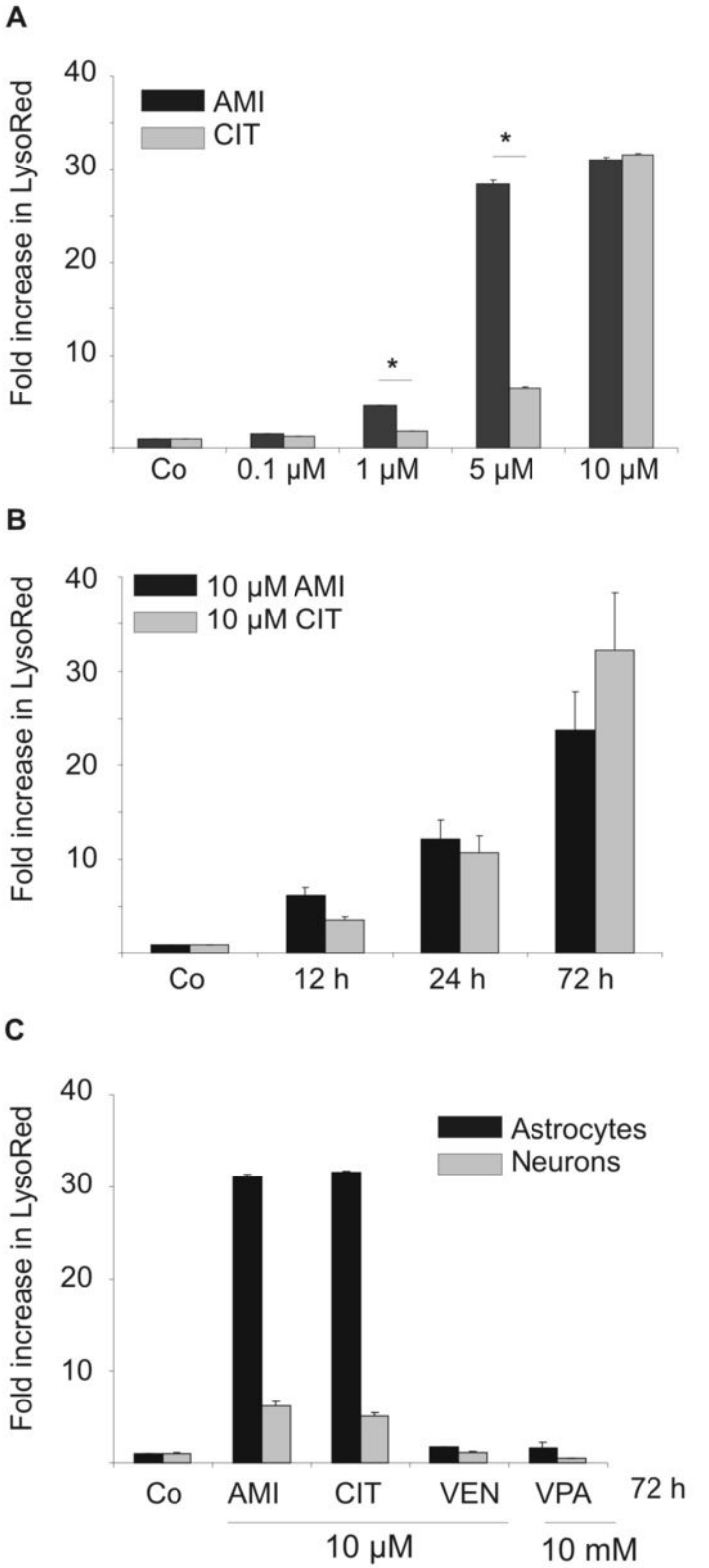
A
Fold increase in LysoRed
40
30
20
10
AMI
CIT
*
*
Co
0.1 μM
1 μM
5 μM
10 μM
B
Fold increase in LysoRed
40
30
20
10
10 μM AMI
10 μM CIT
Co
12 h
24 h
72 h
C
Fold increase in LysoRed
40
30
20
10
Astrocytes
Neurons
Co
AMI
CIT
VEN
VPA
72 h
10 μM
10 mM

Figure 4

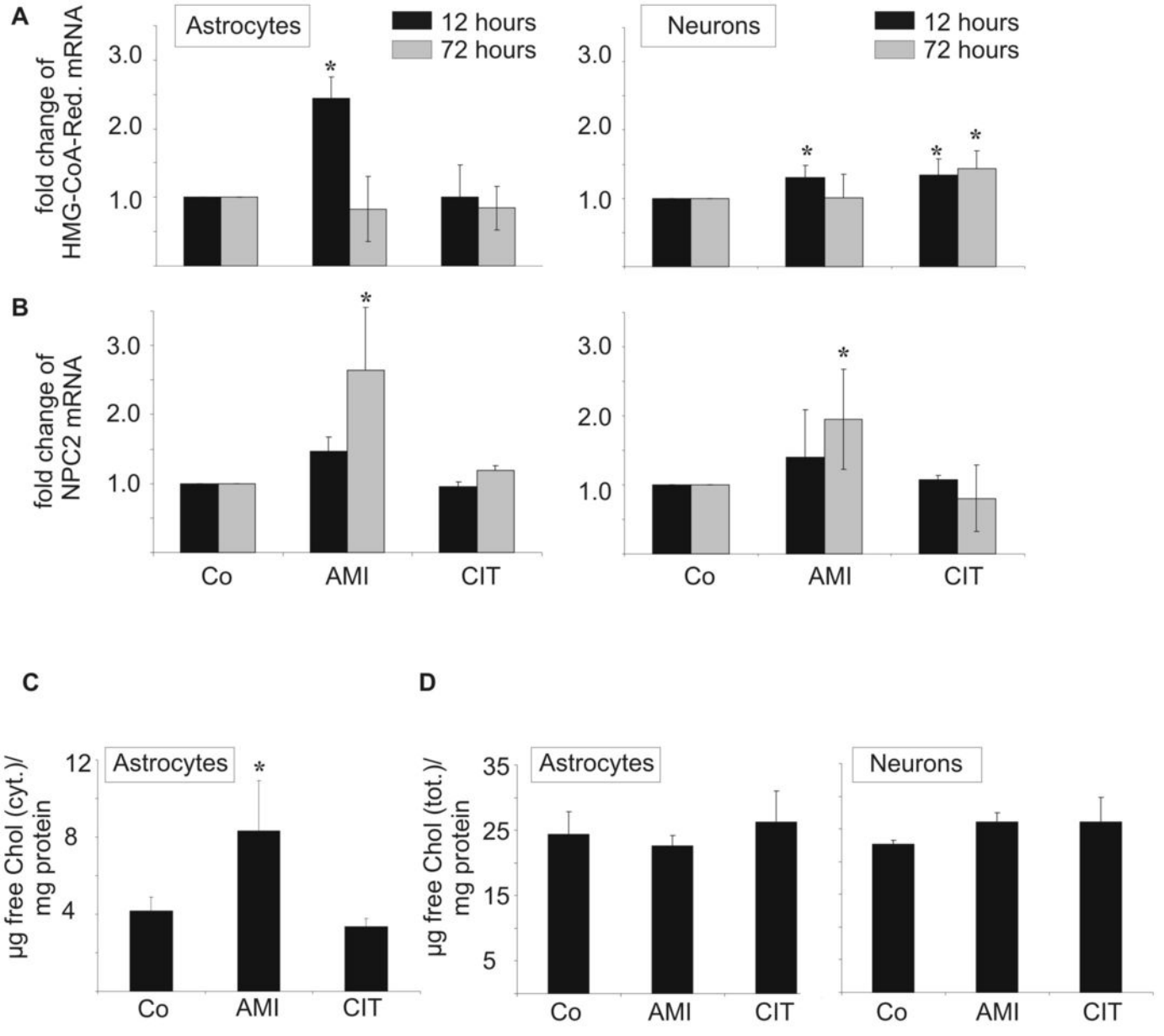
A
Astrocytes
12 hours
72 hours
fold change of HMG-CoA-Red. mRNA
3.0
2.0
1.0
*
Neurons
12 hours
72 hours
3.0
2.0
1.0
*
*
*
B
fold change of NPC2 mRNA
3.0
2.0
1.0
*
Co
AMI
CIT
3.0
2.0
1.0
*
Co
AMI
CIT
C
µg free Chol (cyt.)/ mg protein
12
8
4
Astrocytes
*
Co
AMI
CIT
D
µg free Chol (tot.)/ mg protein
35
25
15
5
Astrocytes
Co
AMI
CIT
Neurons
Co
AMI
CIT

Figure 5

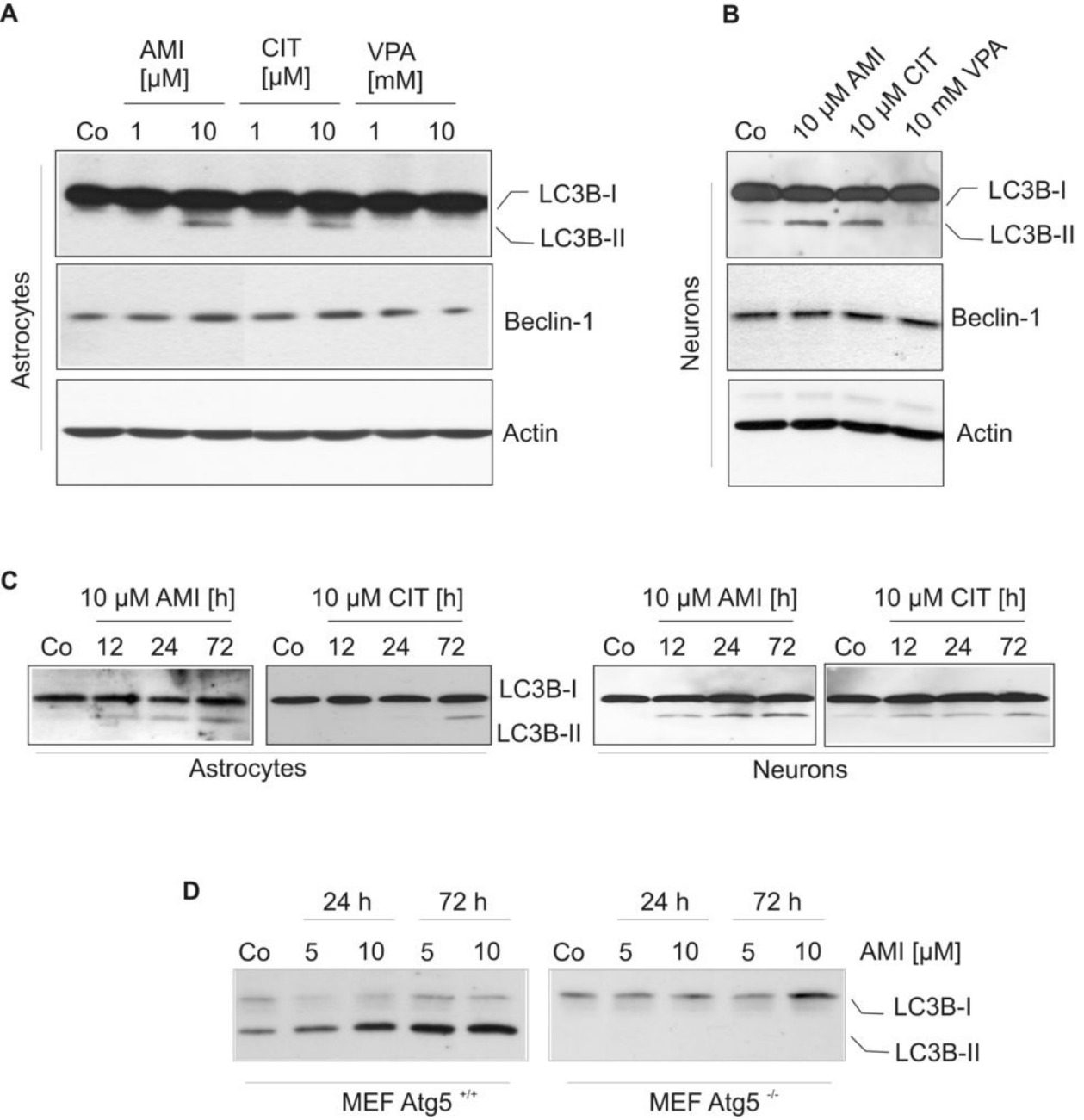
A
AMI [μM]
CIT [μM]
VPA [mM]
Co 1 10 1 10 1 10
LC3B-I
LC3B-II
Beclin-1
Actin
Astrocytes
B
Co 10 μM AMI 10 μM CIT 10 mM VPA
LC3B-I
LC3B-II
Beclin-1
Actin
Neurons
C
10 μM AMI [h]
10 μM CIT [h]
Co 12 24 72 Co 12 24 72
LC3B-I
LC3B-II
Astrocytes
10 μM AMI [h]
10 μM CIT [h]
Co 12 24 72 Co 12 24 72
Neurons
D
24 h 72 h
Co 5 10 5 10 Co 5 10 5 10 AMI [μM]
LC3B-I
LC3B-II
MEF Atg5 +/+
MEF Atg5 -/-

Figure 6

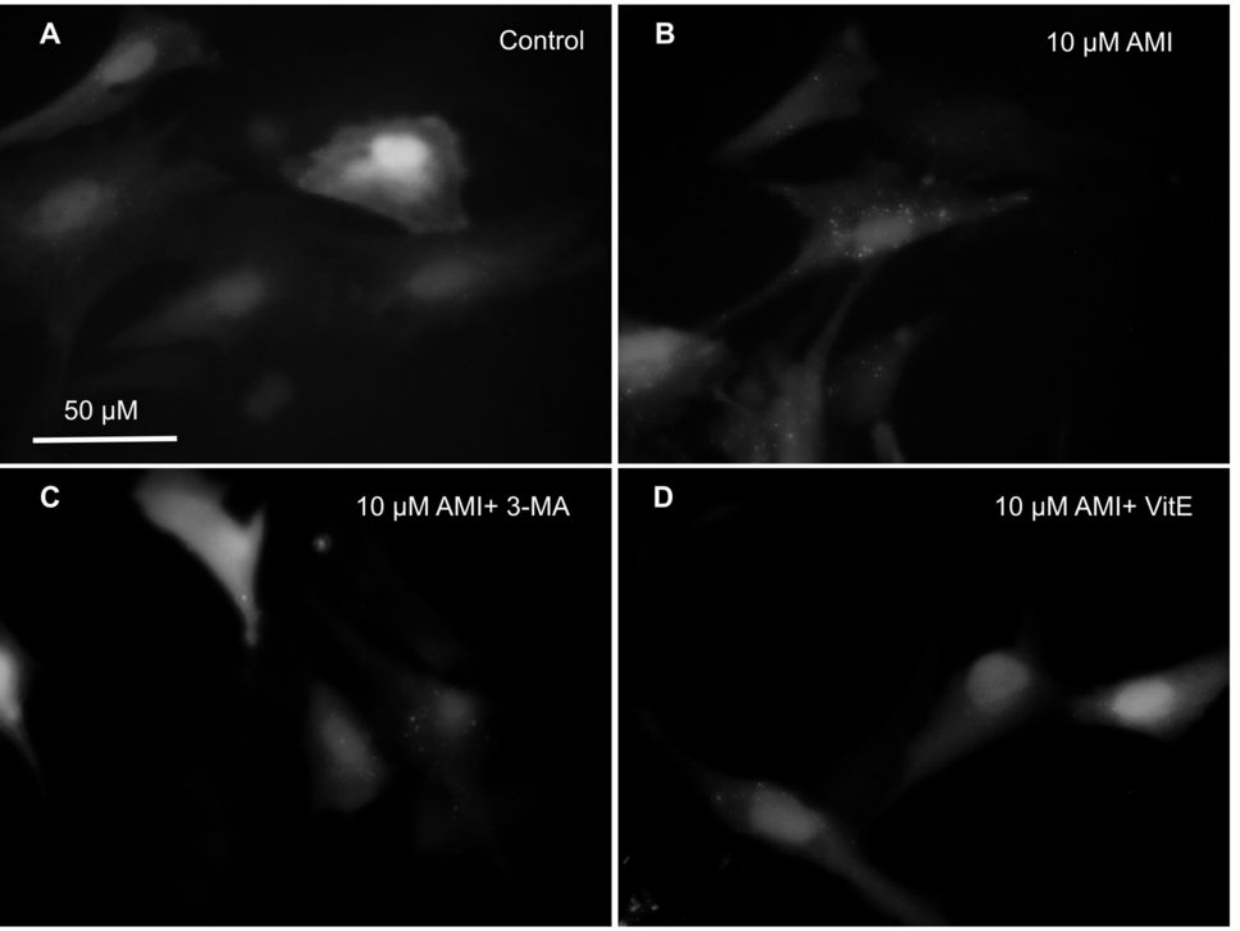
A
Control
B
10 μM AMI
50 μM
C
10 μM AMI+ 3-MA
D
10 μM AMI+ VitE

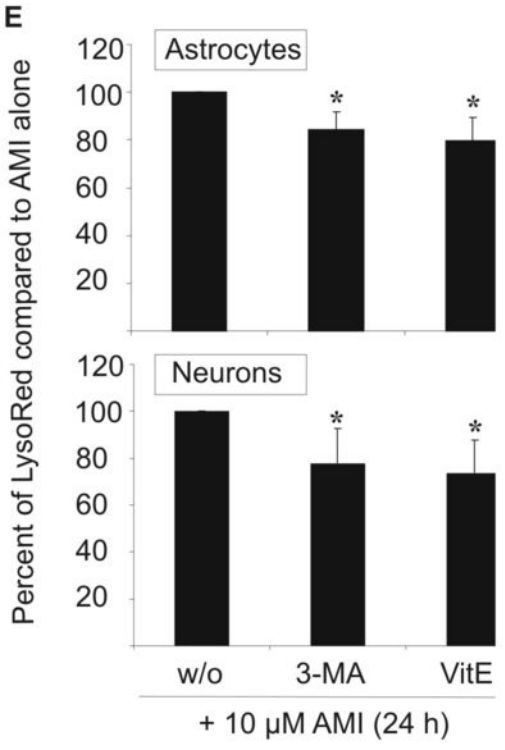
E
Astrocytes
Neurons
Percent of LysoRed compared to AMI alone
120
100
80
60
40
20
*
w/o
3-MA
VitE
+ 10 μM AMI (24 h)

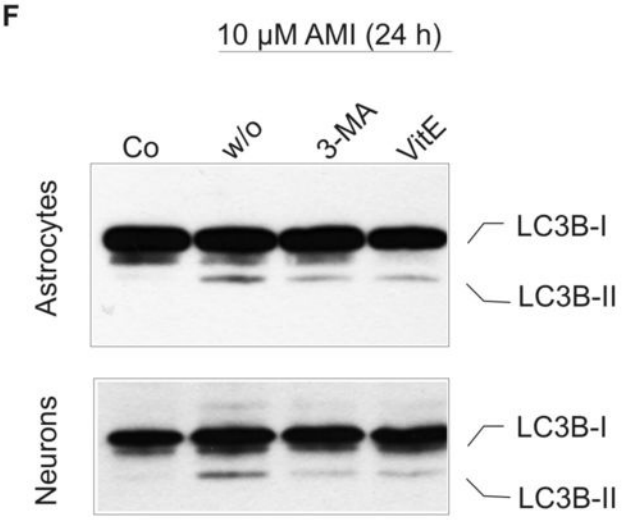
F
10 μM AMI (24 h)
Co
w/o
3-MA
VitE
Astrocytes
Neurons
LC3B-I
LC3B-II

Figure 7

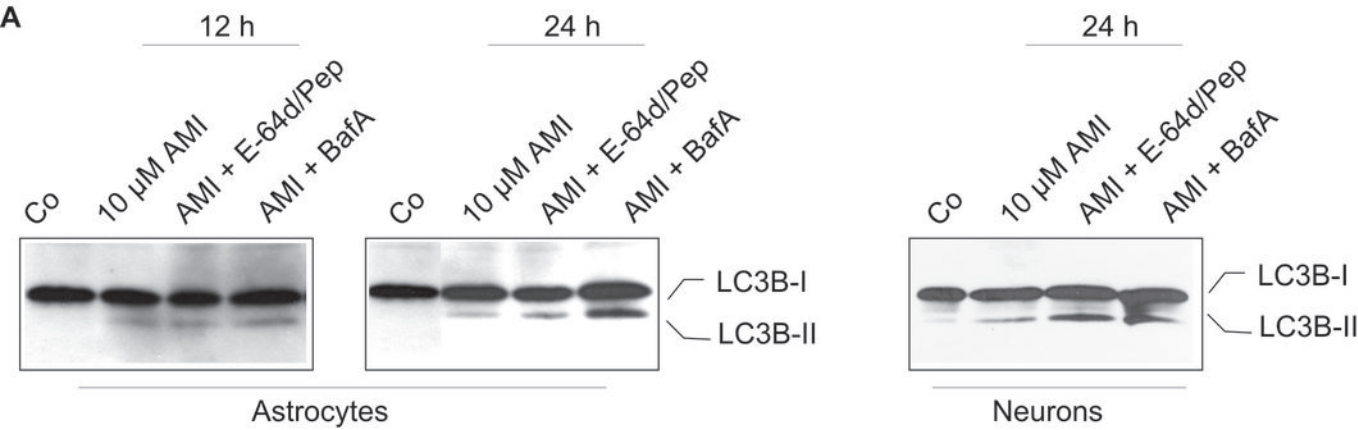
A
12 h
24 h
24 h
Co
10 µM AMI
AMI + E-64d/Pep
AMI + BafA
LC3B-I
LC3B-II
Astrocytes
Neurons

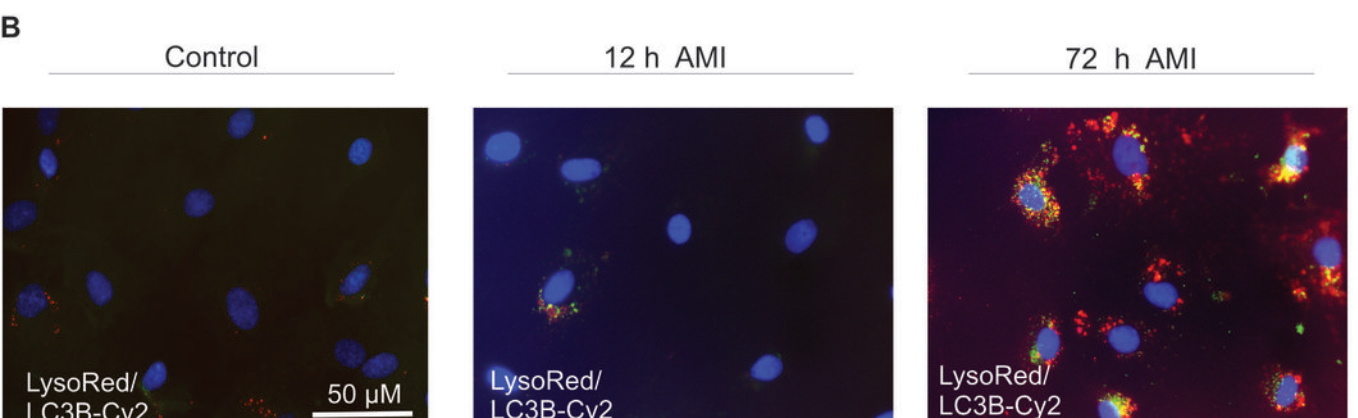
B
Control
12 h AMI
72 h AMI
LysoRed/
LC3B-Cy2
50 µM

Figure 8

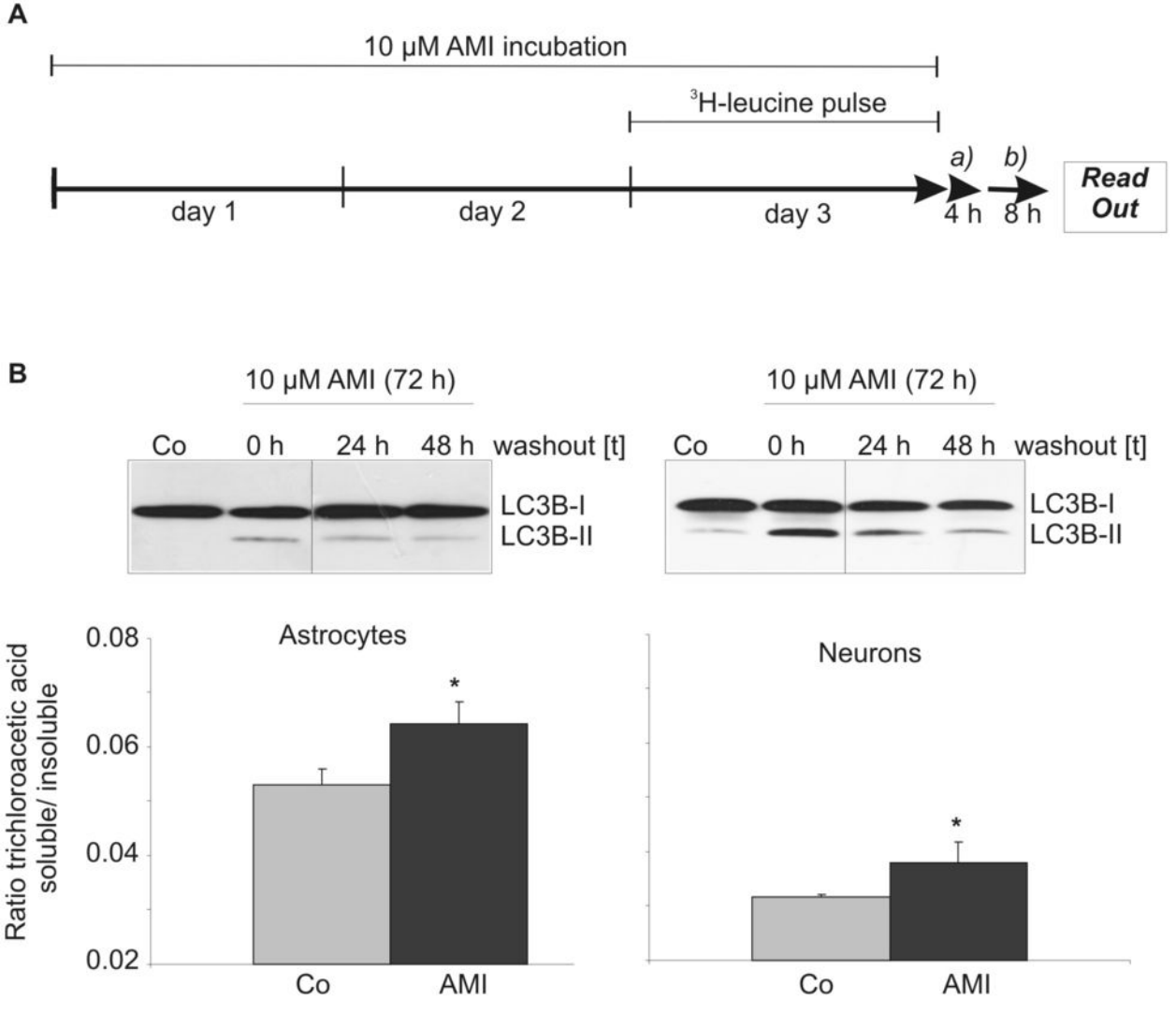
A
10 µM AMI incubation
^{3}H-leucine pulse
a)
b)
Read Out
day 1
day 2
day 3
4 h
8 h
B
10 µM AMI (72 h)
Co
0 h
24 h
48 h
washout [t]
LC3B-I
LC3B-II
10 µM AMI (72 h)
Co
0 h
24 h
48 h
washout [t]
LC3B-I
LC3B-II
Astrocytes
Neurons
Ratio trichloroacetic acid soluble/ insoluble
0.08
0.06
0.04
0.02
*
*
Co
AMI
Co
AMI

Figure 9

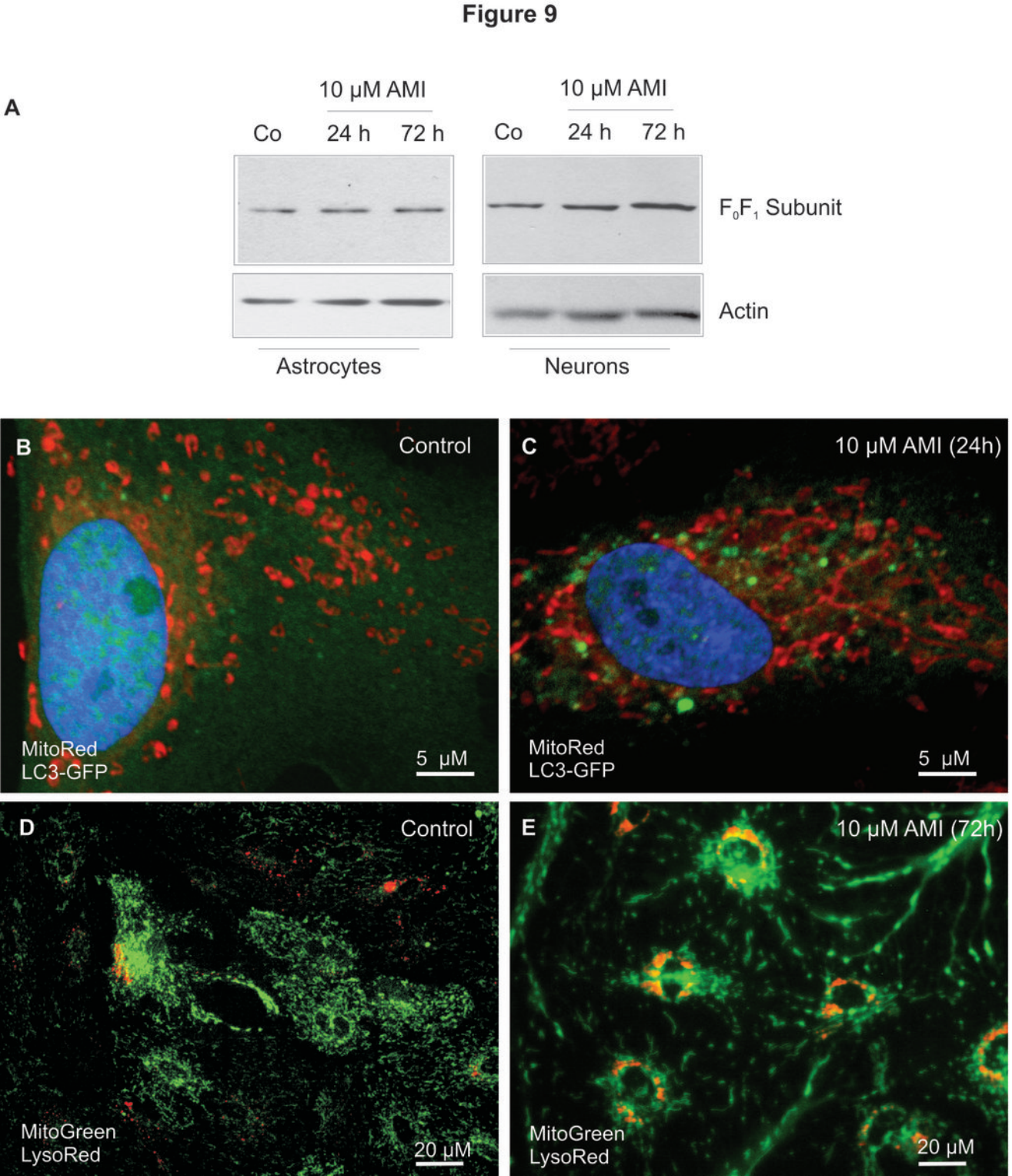
A
10 μM AMI
10 μM AMI
Co
24 h
72 h
Co
24 h
72 h
F_0F_1 Subunit
Actin
Astrocytes
Neurons
B
Control
MitoRed
LC3-GFP
5 μM
C
10 μM AMI (24h)
MitoRed
LC3-GFP
5 μM
D
Control
MitoGreen
LysoRed
20 μM
E
10 μM AMI (72h)
MitoGreen
LysoRed
20 μM

Figure 10

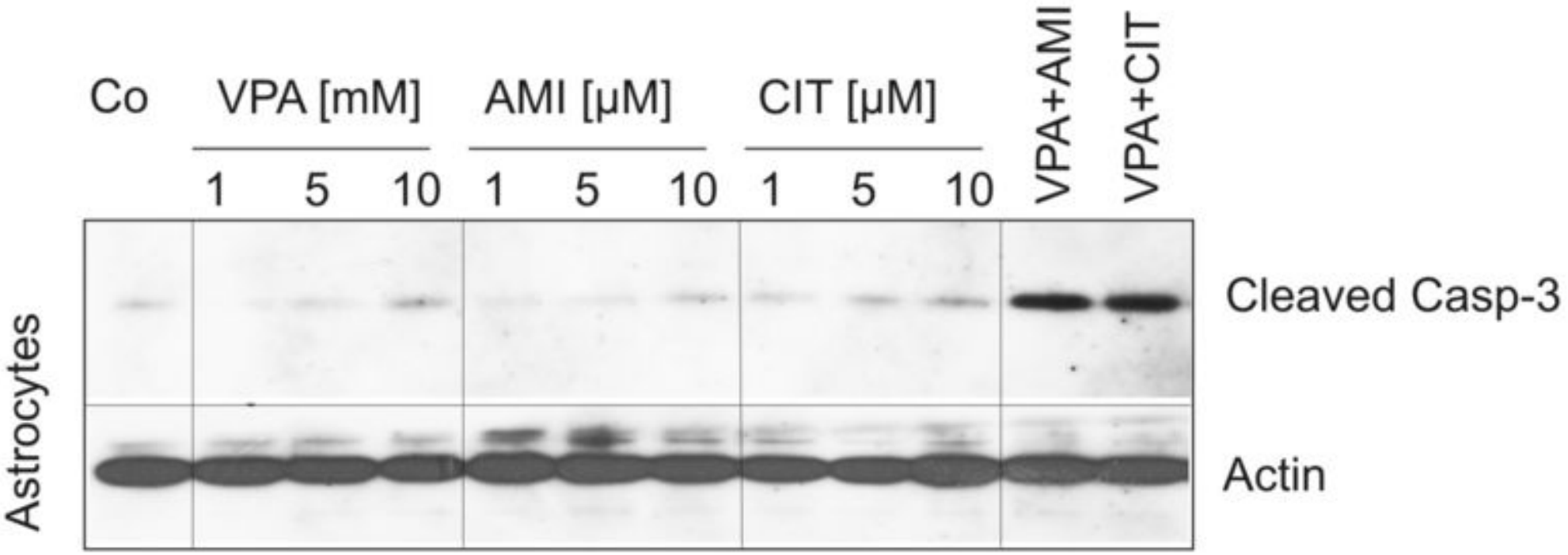
Co
VPA [mM]
AMI [µM]
CIT [µM]
1
5
10
1
5
10
1
5
10
VPA+AMI
VPA+CIT
Astrocytes
Cleaved Casp-3
Actin

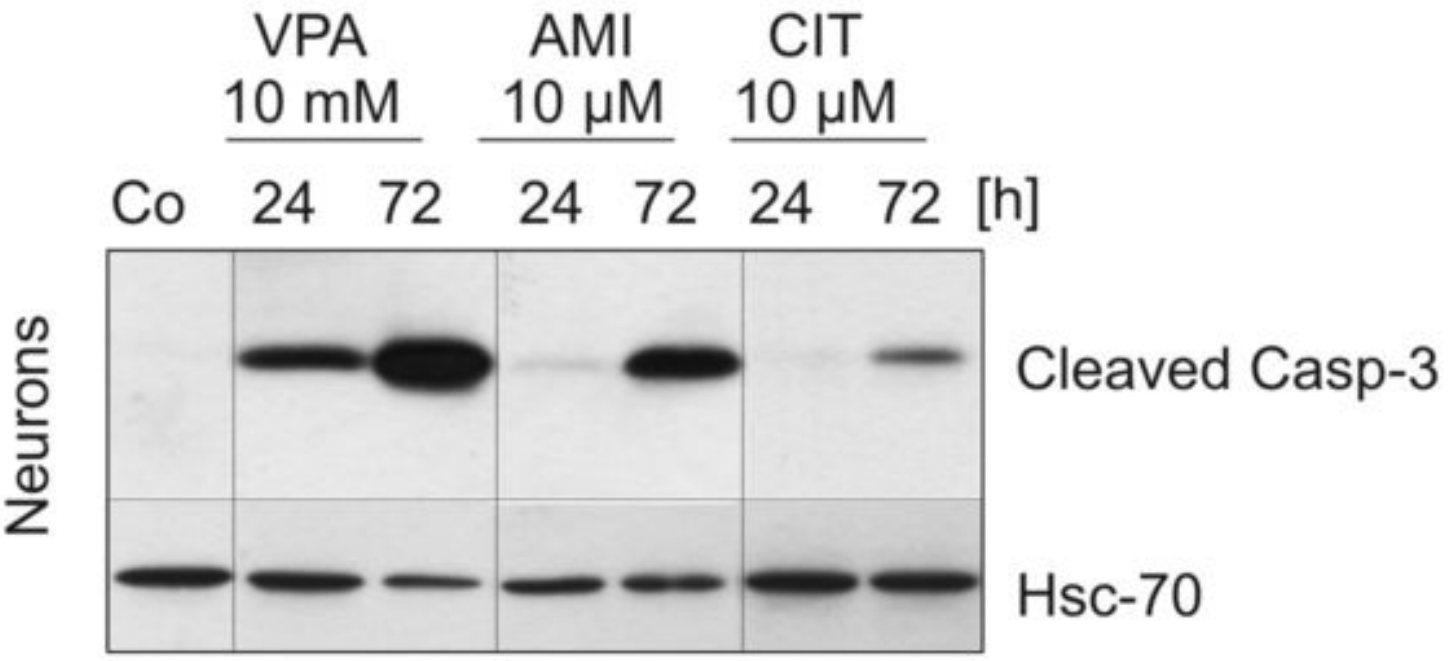
VPA
10 mM
AMI
10 µM
CIT
10 µM
Co
24
72
24
72
24
72
[h]
Neurons
Cleaved Casp-3
Hsc-70

Figure 11

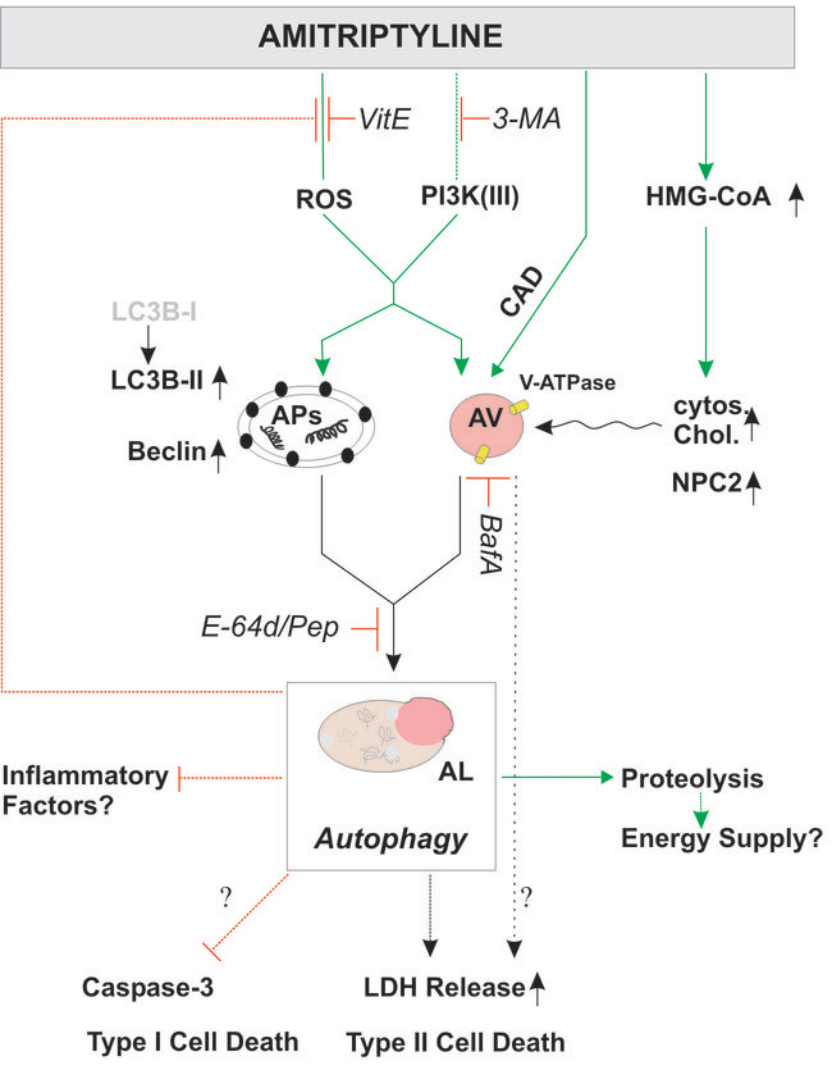
AMITRIPTYLINE
VitE
3-MA
ROS
PI3K(III)
HMG-CoA
CAD
LC3B-I
LC3B-II
APs
Beclin
V-ATPase
AV
cytos. Chol.
NPC2
BafA
E-64d/Pep
AL
Autophagy
Inflammatory Factors?
Proteolysis
Energy Supply?
?
?
Caspase-3
LDH Release
Type I Cell Death
Type II Cell Death